



---

## **Mid-Level Dry Air Intrusions: Regulatory Mechanisms and Impact on Southern Maritime Continent Rainfall**

Ashar A. Aslam<sup>a\*</sup>, Juliane Schwendike<sup>a</sup>, Simon C. Peatman<sup>a</sup>, Cathryn E. Birch<sup>a</sup>, Massimo A.

Bollasina<sup>b</sup> and Paul Barrett<sup>c</sup>

<sup>a</sup>*School of Earth and Environment, University of Leeds, UK*

<sup>b</sup>*School of Geosciences, University of Edinburgh*

<sup>c</sup>*Met Office, Exeter, UK*

\*Correspondence to: A. A. Aslam, School of Earth and Environment, University of Leeds, LS2 9JT, UK.

E-mail: eaaaas@leeds.ac.uk

---

Patterns in extreme precipitation across the Maritime Continent are modulated by many processes, from large-scale modes of variability and planetary waves, to finer-scale processes such as the diurnal cycle. Transient mid-level dry air intrusions are an example of a process not extensively studied over the Maritime Continent.

Through Lagrangian trajectory and event composite analyses, we use a specific humidity metric which identifies mid-level dry air intrusions. These intrusions originate from upper-level disturbances along the subtropical jet. Mid-level cyclonic (anticyclonic) circulation anomalies northwest of Australia in DJF (JJA) intensify westerlies (easterlies) in the southern Maritime Continent, advecting dry air eastward (westward). Such regulatory mechanisms may be linked to the Madden-Julian Oscillation. The resultant transport direction of associated air parcels is also dependent on seasonal low-level monsoon circulation, and potentially convective entrainment.

Dry air suppresses rainfall over the ocean in both seasons. Further suppression matches intrusions trajectories, such as over southern Maritime Continent islands in DJF, and the Indian Ocean in JJA. In both seasons, there is enhanced rainfall to the east of the intrusion, where there is moist return flow to the extratropics. ~~Therefore, dry air intrusions are important in influencing local wind circulations and rainfall patterns in the southern Maritime Continent.~~

*Key Words:* Dry air intrusions, Maritime Continent, rainfall, deep convection, tropical-extratropical interactions

*Received...*

## 1. Introduction

The Maritime Continent (MC) in Southeast Asia consists of an archipelago of thousands of islands and ~~many~~ shallow seas (Figure 1a). High sea surface temperatures (SSTs) and variable topography mean that the MC has an environment conducive of ~~forming~~ deep convection all year round. Rainfall over the MC (Figures 1b–c) is twice the global mean (Yamanaka et al., 2018), with mean precipitation rate ~~exceeding~~  $10 \text{ mm day}^{-1}$  (Ichikawa and Yasunari, 2006). Latent heat release from this precipitation influences global atmospheric circulation and climate through Rossby wave responses (Jin and Hoskins, 1995). The MC has therefore been termed an ‘atmospheric boiler box’ (Ramage, 1968).

Deep convection in the MC forms on multiple spatial and temporal scales, and many processes modulate patterns in precipitation. These processes include the diurnal cycle of solar heating (e.g. Mori et al., 2004; Qian, 2008; Yokoi et al., 2017), large-scale modes of variability such as the Madden-Julian Oscillation (e.g. Madden and Julian, 1971, 1972; Wheeler and Hendon, 2004; Zhang, 2005), El Niño Southern Oscillation (e.g. Haylock and McBride, 2001; Rauniyar and Walsh, 2013), Indian Ocean Dipole (e.g. Saji et al., 1999; Saji and Yamagata, 2003), and planetary waves (e.g. Wheeler and Kiladis, 1999; Yang et al., 2003; Ferrett et al., 2020). Scale interactions also exist between processes, adding further variability to, and therefore complexity to our understanding of, convective organisation, water vapour profiles and cloud structure over the MC (e.g. Rauniyar and Walsh, 2013; Peatman et al., 2014, 2021). Limitations in our knowledge of these processes mean errors exist in model representation of MC precipitation (e.g. Yang and Slingo, 2001; Neale and Slingo, 2003; Qian, 2008; Birch et al., 2016; Vincent and Lane, 2016).

Many ~~other~~ complex fine- and synoptic-scale processes ~~modulate~~ MC precipitation patterns, including tropical cyclones (e.g. Scoccimarro et al., 2020), and interactions between the tropics and the extratropics, such as cold surges (e.g. Fauzi and Hidayat, 2018; Nugroho et al., 2019). Another form of ~~these~~ tropical-extratropical interactions ~~are~~ dry air intrusions, which are dipping tongues of low humidity and high potential vorticity

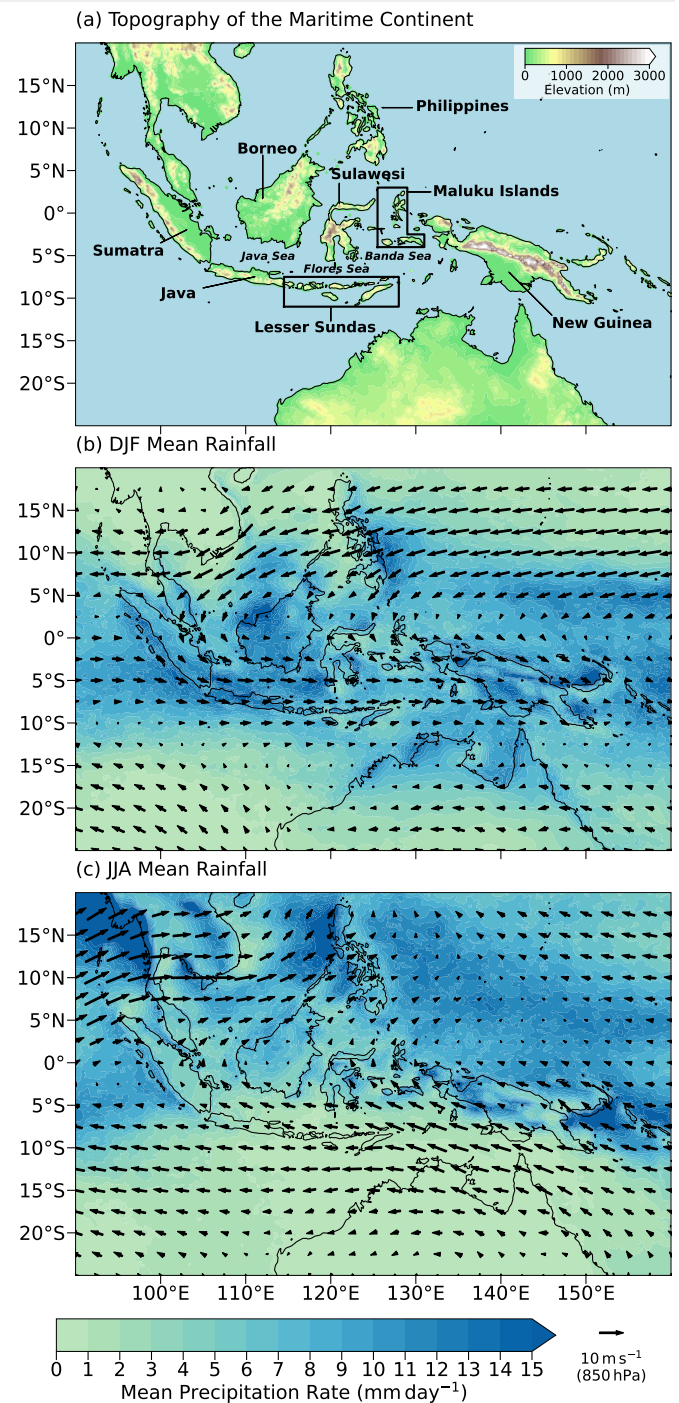


**Figure 1.** (a) Map showing the topography/elevation of the Maritime Continent, with some of its constituent islands and seas labelled. Below panel (a) are climatological means of GPM precipitation rates for (b) DJF and (c) JJA, from 2000/01 to 2019/20. Black arrows represent 850 hPa wind.

(PV) air, 100s of kilometres in width, injected from the upper-troposphere/lower-stratosphere (Danielsen, 1968; Appenzeller and Davies, 1992; Browning, 1997; Stohl, 2001; Zachariasse et al., 2001; Raveh-Rubin, 2017).

Extratropical wave trains act as a source of dry air intrusions, as shown by back trajectory analysis (e.g. Casey et al., 2009) and neural networks (Silverman et al., 2021). Amplification of disturbances along the upper-level subtropical jet, through meridional mixing of PV (Hoskins et al., 2003), causes

instabilities to develop. Intensification of these disturbances leads to isentropic folding of the tropopause and anticyclonic Rossby wave breaking, forcing descent of upper-level dry air (Numaguti, 1995; Bithell et al., 1999; Funatsu and Waugh, 2008; Li et al., 2015). Resultant transport direction of dry air depends on jet position, the background wind field, and small-scale triggers such as changes in rainfall patterns, SSTs and wind (Sheu and Liu, 1995; Krishnamurti et al., 2010; Homeyer and Bowman, 2013; Deng et al., 2018).

Dry air intrusion frequency is variable depending on global location. Waugh and Polvani (2000), Stohl (2001), Casey et al. (2009) and Raveh-Rubin (2017) produced climatologies of dry air intrusion occurrence, defining intrusions through their characteristic humidity and vertical descent anomalies. Dry air intrusions are most prevalent over the Pacific and Indian Ocean, occurring more often in the winter season for each hemisphere. However, they contribute to anomalously dry air all year round.

Atmospheric soundings show dry air intrusions sit atop sharp stable layers, produced by anomalous longwave cooling of the top of the underlying moist air (Mapes and Zuidema, 1996; Zhang and Chou, 1999; Johnson et al., 2001). Dry air intrusions therefore disrupt the tropical atmosphere in reaching radiative-convective equilibrium, having to adjust to humidity fluctuations originating from high-latitudes (Brown and Zhang, 1997; Ryoo et al., 2008). These induced changes to the moisture field, as well as low-latitude circulation, impact regional meteorology and environmental state (e.g. Rodwell, 1997; Knippertz, 2007).

Localised, transient breaks in tropical precipitation on daily-weekly timescales can be associated with dry air intrusion. This link has been observed in regions such as the tropical West Pacific during the Tropical-Ocean Global-Atmosphere Coupled Ocean-Atmosphere Response Experiment (TOGA COARE; e.g. Mapes and Zuidema, 1996; Yoneyama and Parsons, 1999; Lucas and Zipser, 2000; Lucas et al., 2000; Parsons et al., 2000) and Indian subcontinent such as through the INCOMPASS project (e.g. Parsons et al., 2000; Parker et al., 2016; Fletcher et al., 2020; Volonté et al., 2020). These impacts on rainfall and convection are unique, and cannot be consistently predicted by connections to other processes such as the large-scale modes of variability (Krishnamurti et al., 2010).

Mid-level dry air intrusions overrun and cap the moist boundary layer (BL), decreasing BL parcel buoyancy and increasing convective inhibition (CIN). Gradual increases in BL equivalent potential temperature and potential instability lead to convective available potential energy (CAPE) build-up (Brown and Zhang, 1997; Yang et al., 2009; Parker et al., 2016). Increases in CAPE allows convection to erode the dry air layer, primarily through convective cloud detrainment. This process is quickest near intrusion margins where there is less CIN. Though the lower-mid-troposphere can return to moist conditions within a week, the upper-atmosphere may remain anomalously dry for up to 3 weeks (Parsons et al., 2000; Casey et al., 2009). Convective recovery is, however, non-steady, influenced by factors such as mid-latitude dynamics, transient weather systems, the diurnal cycle, orography, convective structure, surface feedbacks, synoptic circulations, and generation of mixing eddies (Mapes and Zuidema, 1996; Brown and Zhang, 1997; Redelsperger et al., 2002; Fletcher et al., 2018; Volonté et al., 2020; Ahmed and Neelin, 2021).

Dry air intrusions can also result in low-level convergence, vertical motion and increased convection when encountering warm, moist air masses on eastward margins and leading edges (Dixon et al., 2003; Hoskins et al., 2003), through advection of cyclonic vorticity, isentropic displacement and reductions in stability ahead of upper-level troughs (e.g. Funatsu and Waugh, 2008; van der Wiel et al., 2015; Vaughan et al., 2017). Dry air intrusions therefore steer and organise deep convection (Tompkins, 2001), leading to localised bursts in rainfall (e.g. Berry and Reeder, 2016). However, the environment near to the intrusion must be moist enough to be conducive of forming deep convection (Pohl et al., 2009; van der Wiel et al., 2015; de Vries et al., 2016, 2018; Kumar et al., 2019). Dry air intrusions must also penetrate deep enough into the lower-troposphere to instigate the moisture flux enabling convection downstream, as they themselves modify the lower-level wind field (Rodwell, 1997; Knippertz, 2007; Ward et al., 2021).

Despite insight gained from past research, dry air intrusions have not been extensively studied in relation to MC precipitation. Murata et al. (2006) and Seto et al. (2006) used rawinsonde, radar and surface meteorological data and identified dry air intrusions over Sumatra. Murata et al. (2006) noted events where there is

convective suppression behind eastward-propagating squall lines. Seto et al. (2006) found this suppression to be associated with intensification of westerly winds. More recently, Feng et al. (2021) used the Sumatran GPS array to investigate summer intraseasonal variability in precipitable water vapour. Dry air intrusions over Sumatra were associated with interactions linked to Rossby waves propagating in the Southern Hemisphere mid-latitudes. However, these studies use few events in their analysis and do not explicitly analyse impacts on rainfall in the region.

Rodwell (1997) highlights that limits to the accuracy of forecasts and predictability of rainfall can be influenced by synoptic-scale/transient events such as dry air intrusions, particularly if a single event provides significant contributions to the seasonal anomaly. These induced anomalies could render an accurate seasonal forecast of monsoon rainfall to be an impossible objective. Further research into processes regulating regional precipitation will benefit society in the MC as communities experience serious floods and landslides as a result of extreme weather. Better meteorological understanding will improve forecasting potential and ensure socioeconomic security for the 400 million people living in the MC, alleviating current vulnerability to disaster and loss (Wijayanti et al., 2017; Narulita and Ningrum, 2018).

In this study, we use 42 years of ERA5 reanalysis data to identify dry events near the MC through analysis of variance and anomalies in humidity. Section 2 outlines methods used, including utilised data, the workflow in identifying dry events and computation of air parcel trajectories to determine attribution to dry air intrusions. We present results in Section 3, including parcel trajectories, regulatory mechanisms of mid-level dry events, and impacts on regional rainfall patterns. Section 4 synthesises these results to see if there are similarities between this work and past studies, or whether processes and impacts related to dry events are unique for this region. Conclusions are provided in Section 5.

## 2. Methods

### 2.1. Data

ERA5 data, the fifth generation ECMWF reanalysis of global climate and weather (Hersbach et al., 2020), is used in

this work. ~~Single level and multi level (37 levels) data, on several atmospheric, land and ocean parameters with uncertainty estimates, is available hourly. Data covers the globe at around 26 km grid spacing ( $0.25^\circ \times 0.25^\circ$ ), resolving the atmosphere up to 80 km. ERA5 covers the period from 1950 present, extended continuously in time with daily updates a few days behind real-time, and quality assured monthly updates within 3 months of real-time. Data assimilation and modelling schemes are employed to keep ingested observational data from a wide range of historical observations to within uncertainty.~~ The Copernicus Climate Data Store was accessed to download ERA5 data from 1979 to 2021 (42 years) for 20 levels from 50 hPa to 1000 hPa at 50 hPa resolution, using the domain of  $20^\circ\text{N}$ - $60^\circ\text{S}$ ,  $60^\circ$ - $160^\circ\text{E}$ .

Rainfall data is obtained from the Global Precipitation Measurement (GPM) mission, which has been pre-processed using the Integrated Multi-Satellite Retrievals for GPM (IMERG) Version 06 algorithm (Huffman et al., 2020). The GPM mission involves a constellation of satellites from various nations, with combined data offering accurate and fine spatial ( $0.1^\circ \times 0.1^\circ$ ) and temporal (30 min) resolution of precipitation estimates worldwide. The IMERG algorithm inter-calibrates gauge data with precipitation estimates from satellite infrared and microwave sensors. These estimates include those from the GPM and TRMM (Tropical Rainfall Measuring Mission; Simpson et al., 1996) eras. Data is available for all longitudes and for latitudes between  $65^\circ\text{N}$  and  $65^\circ\text{S}$ . Processed daily mean rainfall data was available from June 2000 to August 2021, but 20 years of continuous data from December 2000 to November 2020 is used here.

Daily means were averaged over all years used in this work for each variable to produce a mean annual cycle (366 days in length). This mean annual cycle was smoothed through application of a 15-day moving window.


### 2.2. Dry Event Identification

~~Specific humidity, the mass of water vapour in a unit mass of moist air and therefore an absolute value of moisture content, is used as the key metric for identifying dry air intrusions.~~ Analysis of the variance in daily mean specific humidity at 700 hPa was conducted for each season and across the entire time period of study. A box was selected based on identification

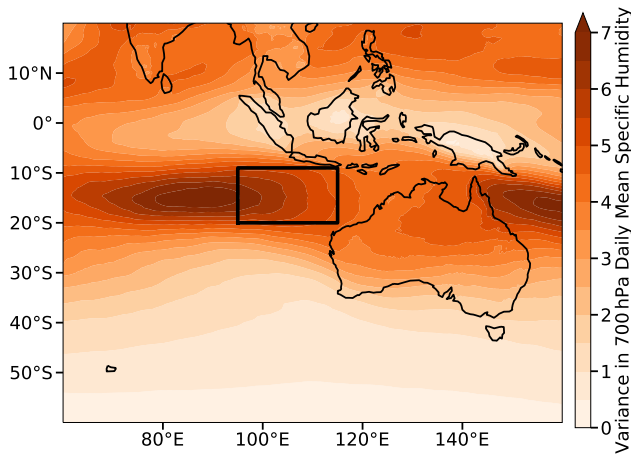


**Figure 2.** Variance in daily mean specific humidity at 700 hPa for the entire time period of analysis from December 1979 to November 2021. The black box (9–20°S, 95–115°E) represents the selected region in this study for identification of mid-level dry events.

of regions of high variance in this metric. As shown in Figure 2, highest variance in mid-level specific humidity is observed either side of the Maritime Continent. Prominent locations of high variance include the eastern Indian Ocean southwest of Sumatra and Java, and the southwestern Pacific Ocean near New Guinea and Australia. A box is selected covering the region of 9–20°S, 95–115°E, near to Sumatra and Java. This covers the eastern periphery of the first high variance region identified, located between 10–20°S and 80–100°E, and is close to the centre of the domain used for data downloads. The position of the box was chosen through a compromise made between variance and proximity to the MC, given the higher variance zone is further out into the Indian Ocean.

For identifying dry air intrusions, 700 hPa specific humidity was averaged over the identifier box for each daily mean and the associated smoothed mean annual cycle value for that day and month. The smoothed mean annual cycle value was subtracted from the daily mean to give an anomaly in specific humidity, normalised relative to the smoothed mean annual cycle. Dry days were defined as days where normalised specific humidity anomalies are more negative than the 5th percentile, computed for each season from 1979/1980 to 2020/21. Therefore, the number of dry days per season is 5% of the number of days across all 42 years for that particular season. If the normalised specific humidity anomalies associated dry days are not exceeded (more negative) by other dry days 10 days either side, they are classed as dry events (later referred to as ‘Day 0’).  is to isolate

events associated with an individual dry air intrusion, ensuring they are not accounted for more than once. Given effects of dry air intrusions are noted up to 8–15 days after an intrusion (in TOGA COARE; e.g. Yoneyama and Fujitani, 1995; Parsons et al., 2000), defining events with a 10-day window either side of a minimum in normalised specific humidity anomalies can be justified. This method also enables more effective compositing of events across a greater timescale.

Though past studies have associated mid-level dry air intrusions with a variety of metrics, most identify dry air intrusions through humidity metrics. Studies of dry air intrusions over the MC conducted by Murata et al. (2006) and Seto et al. (2006) also used humidity, thereby justifying choosing this metric. Singh and Sandeep (2021) used a similar method to the one described above, for studying breaks in the Indian monsoon, where they labelled a maximum in a metric (transport of moisture deficient air to the west of India) as being indicative of a dry air intrusion. Employing our chosen method, we identify 201 dry events over the 42 year period of analysis. For DJF and JJA, we find 47 and 56 dry events for each season respectively.

### 2.3. Trajectory Analysis

The Lagrangian trajectory equation is used to track air parcels associated with dry events and to determine attribution to dry air intrusions. This equation is employed in tools such as HYSPLIT, used particularly for air concentration and pollution studies (e.g. Draxler et al., 1998; Stein et al., 2015), and LAGRANTO, developed initially for analysing the spatiotemporal variability and dynamics of extratropical cyclones, but also used for determining moisture sources and tracking cloud properties (e.g. Wernli and Davies, 1997; Sprenger and Wernli, 2015). Advection of each parcel only requires details of the three-dimensional wind field, used to track the location and physical properties of these particular parcels for time periods of interest. Here, trajectories were computed manually, where a first guess (denoted with a prime symbol) position of a parcel at time  $t + \Delta t$  is

$$\mathbf{r}'_{t+\Delta t} = \mathbf{r}_t + \mathbf{v}_t(\mathbf{r}_t) \cdot \Delta t, \quad (1)$$

where  $\mathbf{r}$  is the three-dimensional spatial co-ordinate  $(x, y, z)$  related to the position of the air parcel, and  $\mathbf{v}$  is the three-dimensional wind velocity field  $(\mathbf{u}, \mathbf{v}, \omega)$  at position  $\mathbf{r}$ , with  $\mathbf{u}$  and  $\mathbf{v}$  in  $\text{m s}^{-1}$  and  $\omega$  in  $\text{Pa s}^{-1}$ .  $\Delta t$  represents the time step, which is -1 (1) day or -86400 (86400) seconds for back (forward) trajectory analysis. An adjusted mean wind is determined from

$$\bar{\mathbf{v}} = 0.5[\mathbf{v}_t(\mathbf{r}_t) + \mathbf{v}_{t+\Delta t}(\mathbf{r}'_{t+\Delta t})], \quad (2)$$

to give the final position of the air parcel

$$\mathbf{r}_{t+\Delta t} = \mathbf{r}_t + \bar{\mathbf{v}} \cdot \Delta t. \quad (3)$$

As ERA5 data offers  $0.25^\circ$  horizontal resolution, and data is downloaded at 50 hPa vertical resolution, when a guess position is not located on these defined grid points or levels, linear interpolation is applied to determine the values of  $\mathbf{v}$  associated with their position  $\mathbf{r}$ . If  $\mathbf{r}$  exists outside the domain ( $20^\circ\text{N}$ - $60^\circ\text{S}$ ,  $60^\circ$ - $160^\circ\text{E}$ ) or hits the surface ( $z > 1000$  hPa) or top of the vertical domain ( $z < 50$  hPa), the trajectory is terminated.

### 3. Results

#### 3.1. Parcel Trajectories

~~In this section, we provide results for trajectory analysis computed using the equations described in Section 2.3.~~ In Figure 3, differences in the distribution of air parcels associated with the trajectories are calculated by taking the DJF distribution of air parcels and subtracting a normalised JJA distribution which accounts for the difference in number of events analysed between the two seasons, and therefore the amount of trajectories. Blue (red) filled contours therefore reflect regions where more DJF (JJA) air parcels are located. Figure 4 provides details on the spatial distribution for where air parcel trajectories terminate both back (a-d) and forward (e-h) in time.

10-15 days before the event, JJA parcels are located **more northern** over the MC between  $0$ - $15^\circ\text{S}$  and  $80$ - $160^\circ\text{E}$ , while DJF parcels are located further south over the Indian Ocean between  $15$ - $35^\circ\text{S}$  and  $60$ - $130^\circ\text{E}$ . (Figure 3a). Going forward in time, average trajectories suggest parcels **most commonly** enter the domain from the upper-troposphere ( $200$ - $500$  hPa) and

extratropics over the southern Indian Ocean to the west (Figures 3b and 4a-d). This is observed most strongly during DJF 5-10 days before the dry event, but also in JJA. Just before the dry event, most DJF parcels are close to the identifier box where trajectories began (Figure 3c). However, JJA distribution suggests parcels can come from the extratropics during up to 5 days before the event, with some advected southwestward from the tropics. The extratropical source to the southwest is however common to both DJF and JJA regardless of how far back in time one goes, though JJA has an additional source coming from the tropics east of New Guinea.

Up to 5 days after the dry event, DJF parcels are mostly advected eastward across the MC towards New Guinea, with some also advected westward (Figures 3d). Up to 10 days after the event, the eastward propagation noted in DJF persists (Figure 3e). The further east a parcel goes in DJF, the more likely it re-ascends to upper-levels (Figure 4e). The smaller proportion of parcels propagating westward also re-ascend. Most DJF air parcels are advected further equatorward, either re-ascending to the upper-levels, or remain confined to the near-surface (Figure 4f). Compared to DJF, JJA parcels are, on average, advected northwest towards India, while some are also advected northeastward over Sumatra and Malaysia towards mainland SE Asia (Figures 3d-f). The small number of JJA parcels which propagate eastward re-ascend gradually to the mid-levels up to around 500 hPa before exiting the domain in the extratropics (Figures 4g-h). However, the majority which are advected westward continue to descend further below 700-800 hPa. These parcels are eventually advected northward, re-ascending to a maximum of around 300 hPa. Parcels propagating further northward across the Equator however remain in the mid-levels or below. Parcels in both seasons which remain in the near-tropics close to the identifier box tend to continue descending towards the surface.

Averaging these distributions across latitude-longitude space, air parcels associated with the trajectories linked to dry events have characteristic vertical descent from 10 days before the event, to 10 days after (Figure 3g). However, DJF parcels, compared to JJA, are sourced from the upper-levels further back in time, taking longer to descend to the mid-levels. After the event, JJA parcels have a stronger descent signal compared to DJF, which has

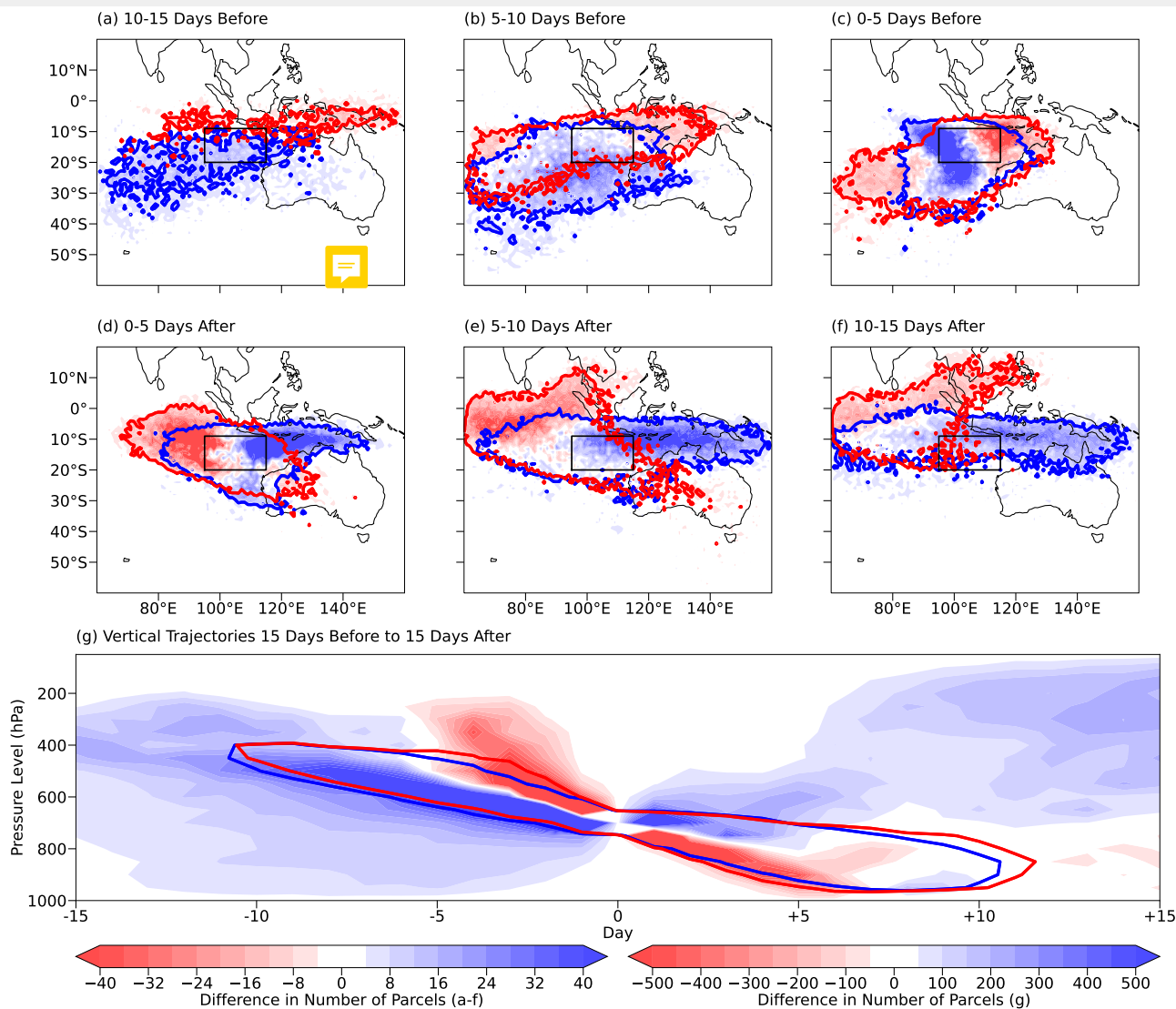


**Figure 3.** Density heatmaps of the difference in air parcel distribution as calculated through (a-c) back and (d-f) forward trajectory analysis, where the difference is equivalent to the JJA distribution subtracted from the DJF distribution. Blue and red filled contours therefore indicate characteristics of the DJF and JJA distributions respectively. Blue and red contours represent the distribution of air parcels within each time range for DJF and JJA, indicated by contours marking 10 parcels. Distributions have been shown in bins of 5 days up to 15 days before or after the dry event, dependent on whether the trajectories analysed go back or forward in time. Panel (g) shows these differences across the pressure levels, averaged over latitude-longitude space, from Day -15 to +15. Blue and red contours represent the 1000 parcel level in terms of the distribution for DJF and JJA respectively. Where differences have been calculated, JJA values have been normalised so that the distribution of parcels is as if there were the same amount of dry events as in DJF (56 compared to 47). Trajectories here are computed for each grid point within the identifier box (9-20°S, 95-115°E) at Day 0, where both latitude and longitude co-ordinates are whole integers (providing 252 trajectories for each event). In the presented figures, trajectory distribution are averaged to the nearest latitude and longitude that is a whole number (a-f) or pressure level that is a multiple of 50 hPa (g) for ease of visualisation.

a broader vertical distribution, linked to an increase in the amount **3.2.1. DJF**

of parcels which end up re-ascending to the upper-levels.

### 3.2. Regulatory Mechanisms

Here, we provide insight into mechanisms regulating dry event occurrence for events identified in DJF and JJA. Figures 5 and 6 show lead-lag composites of specific humidity anomalies for DJF and JJA events, binned into groups of 3 days from Day -7 to Day +4. Figure 7 shows geopotential height Hovmöllers for Days -7 to 0, for both the extratropics and near-tropics (identifier box region).

Up to 7 days before the dry event, a moist anomaly develops over northern Australia (Figure 5a). Mid-level westerly anomalies develop over the southern MC, with a mid-level cyclonic circulation anomaly developing northwest of Australia. Between Days -4 and -2, a dry anomaly develops south of the MC, driven by southerly advection from the extratropics (Figure 5b). At upper-levels, this advection is attributed to disturbances along the subtropical jet, where a cyclonic circulation anomaly develops southwest of Australia, with anticyclonic circulation anomalies either side. These are associated with signals of, predominantly, an upper-level trough in the extratropics, most intense around Day -3

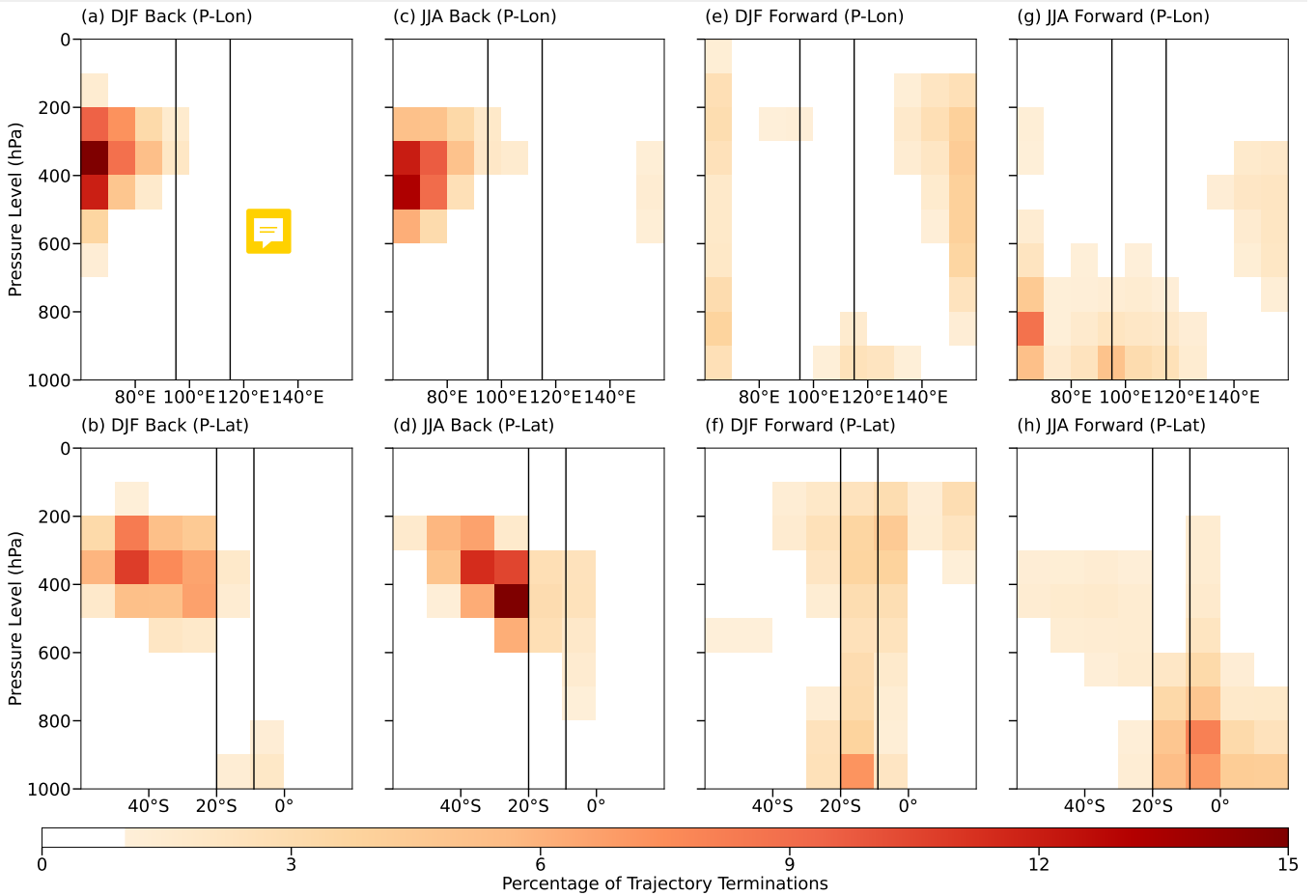


**Figure 4.** Heatmaps showing the spatial distribution of where computed air parcel trajectories terminate both back (a-d) and forward (e-h) in time for DJF (columns 1 and 3) and JJA (columns 2 and 4). Each row represents spatial distributions in pressure-longitude and pressure-latitude space in order from top to bottom. The black boxes or lines represent the spatial limits of the domain used to identify dry events and where trajectories begin for each spatial co-ordinate set.

(Figure 7a). Vertical descent anomalies accompany the southerly advection to the west of the trough. A strong anticyclonic anomaly (ridge) develops to the east over Australia. Mid-level circulation anomalies almost parallel that of the upper-levels, extending further northward towards the MC. These anomalies are linked to a persistent mid-level ridge and trough (Figure 7b). While the ridge does not significantly intensify, the trough deepens around Day -3. Westerlies over the southern MC are enhanced, and the intensified return flow to the extratropics east of the mid-level cyclonic anomaly increases the moist anomaly over Australia.

Around the time of the dry event, while the dry anomaly and vertical descent intensifies, upper-level disturbances in the extratropics dissipate (Figure 5c). However, the anticyclonic circulation anomaly over Australia persists, resulting in a preserved moist anomaly over Australia. The mid-level cyclonic circulation anomaly near to the MC develops a NW-SE tilt, centred just off of northwestern Australia, and the previously enhanced westerlies begin to weaken. Between Days +2 to +4, the dry anomaly begins to dissipate and spreads out longitudinally,

with the moist anomaly over Australia also reduced (Figure 5d). Anomalous mid-level westerlies in the southern MC are weaker than prior to the dry event, linked to the weakened mid-level cyclonic anomaly.

### 3.2.2. JJA

Between Days -7 and -5, a dry anomaly forms to the east of the identifier region over northern Australia and seas adjacent to MC islands (Figure 6a). This anomaly stems from upper-level disturbances further east over eastern Australia, with southeasterly advection towards the MC. However, composite mid-level wind anomalies here are weak. The pre-existing dry air migrates westward over Java, the Lesser Sundas, South Sulawesi, the Maluku Islands, and neighbouring seas (Java and Flores) between Days -4 and -2 (Figure 6b). A new upper-level disturbance develops to the southwest of the identifier box over the southeastern Indian Ocean, leading to southerly-to-southeasterly advection at both upper- and mid-levels. This advection is linked



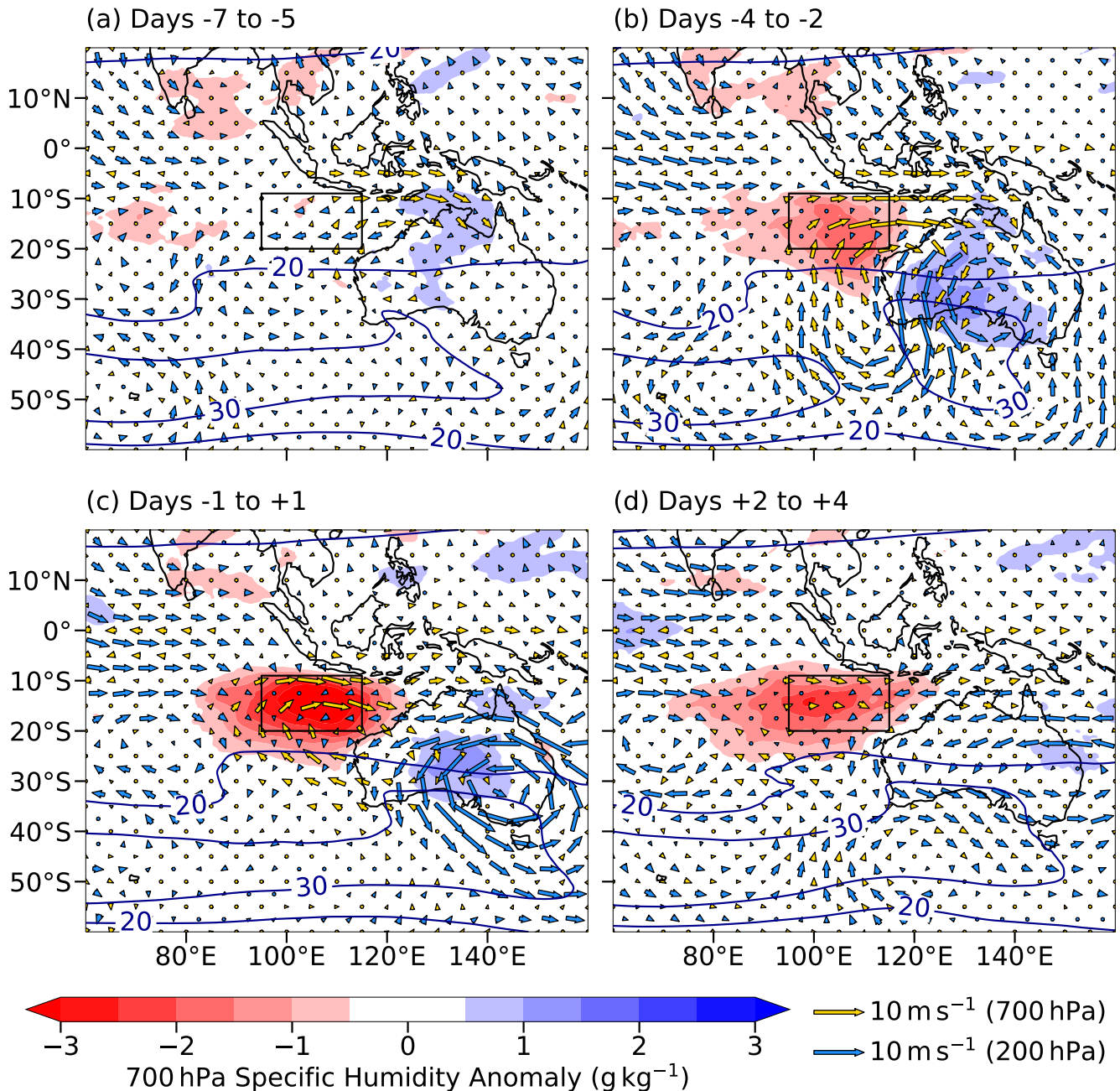


**Figure 5.** Lead-lag composites for 700 hPa specific humidity anomalies for the 47 dry events identified in DJF from 1979/80 to 2020/21. These are grouped into bins three days in size: (a) Days -7 to -5, (b) Days -4 to -2, (c) Days -1 to +1 and (d) Days +2 to +4. Yellow and blue arrows represent 700 hPa and 200 hPa anomalous wind relative to climatology respectively. Blue contours represent 200 hPa wind at the  $20 \text{ m s}^{-1}$  and  $30 \text{ m s}^{-1}$ , indicating the position of the DJF subtropical upper-level jet. The black box represents the domain used for identifying dry events as in Figure 2.

to an anticyclonic circulation anomaly, attributed to an upper-level ridge (Figure 7c), intensifying easterlies at mid-levels to the west of the MC, as well as dry air advection into the tropics. Adjacent to this ridge is a comparably weaker trough, with a vertical descent signal between these anomalies. Similarly, a mid-level ridge develops around Day -3 leading to vertical descent and southeasterly advection to the east (Figure 7d).

Around Day 0, strong upper-level anticyclonic and cyclonic circulation anomalies are observed to the west and over Australia respectively (Figure 6c), linked to continued strengthening of

upper-level geopotential height anomalies (Figure 7c). The mid-level ridge parallels this motion and extends into the tropics, increasing the intensity of the dry anomaly - this trough is of similar intensity to the neighbouring ridge to the west (Figure 7d). The dry anomaly is centred to the south of the MC, though is spread over Java and adjacent seas, due to pre-existing dry air advected from the east. The mid-level circulation anomaly is tilted NW-SE, with moist anomalies either side of the dry anomaly of similar tilt. The days following the dry event are associated with dissipation of upper-level anomalies near the tropics, with propagation of anomalies further to the east (Figure 6d). These

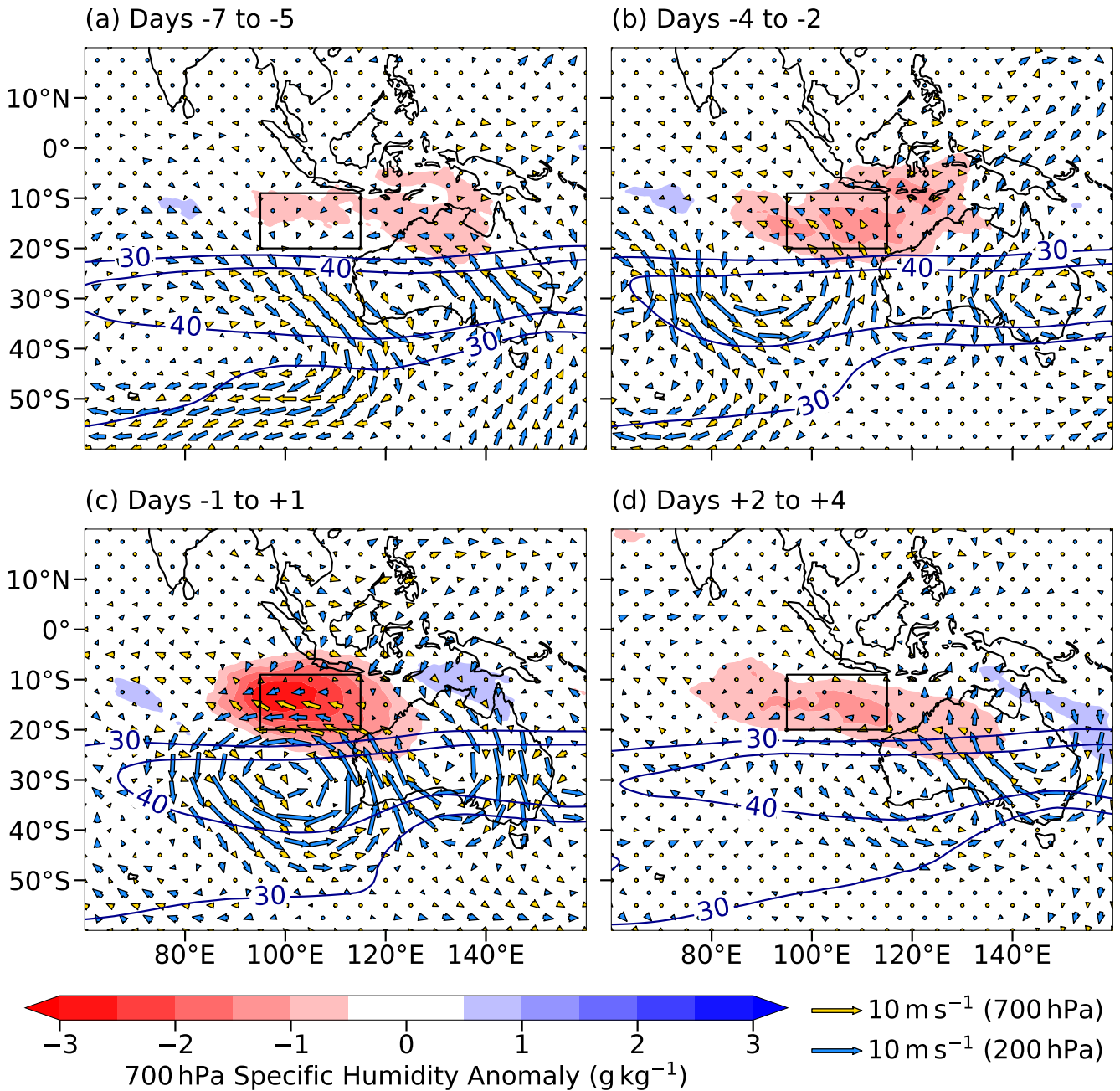


**Figure 6.** Lead-lag composites for 700 hPa specific humidity anomalies for the 56 dry events identified in JJA from 1979/80 to 2020/21. These are grouped into bins three days in size: (a) Days -7 to -5, (b) Days -4 to -2, (c) Days -1 to +1 and (d) Days +2 to +4. Yellow and blue arrows represent 700 hPa and 200 hPa anomalous wind relative to climatology respectively. Blue contours represent 200 hPa wind at the  $30 \text{ m s}^{-1}$  and  $40 \text{ m s}^{-1}$ , indicating the position of the JJA subtropical upper-level jet. The black box represents the domain used for identifying dry events as in Figure 2.

anomalies lead to a new stream of anomalous dry air passing over Australia. Dry air originally near to the MC spreads out longitudinally, and the moist anomaly has propagated further east.

### 3.2.3. Summary

Results here show that upper-level disturbances within the subtropical jet, developing around 5 days prior to the dry event, are a key precursor to dry event occurrence in both seasons. These disturbances drive vertical descent of dry air towards the tropics. However, enhancement in mid-level cyclonic circulation centred over northwestern Australia strengthens mid-level southerlies

in DJF, enabling advection of dry air towards the MC. This circulation also produces anomalous southern MC westerlies which advect dry air eastward. On the other hand in JJA, an enhancement in mid-level anticyclonic circulation just to the west of Australia strengthens mid-level southerlies, though directing dry air to the same region as in DJF. This circulation too enhances easterlies south of the MC which advects dry air westward towards the Indian ocean. For both seasons, these dry events can therefore be associated with dry air intrusions. Gradual weakening of enhanced wind circulations in DJF and JJA lead to eventual dissipation of the dry anomalies. In both seasons, moist anomalies

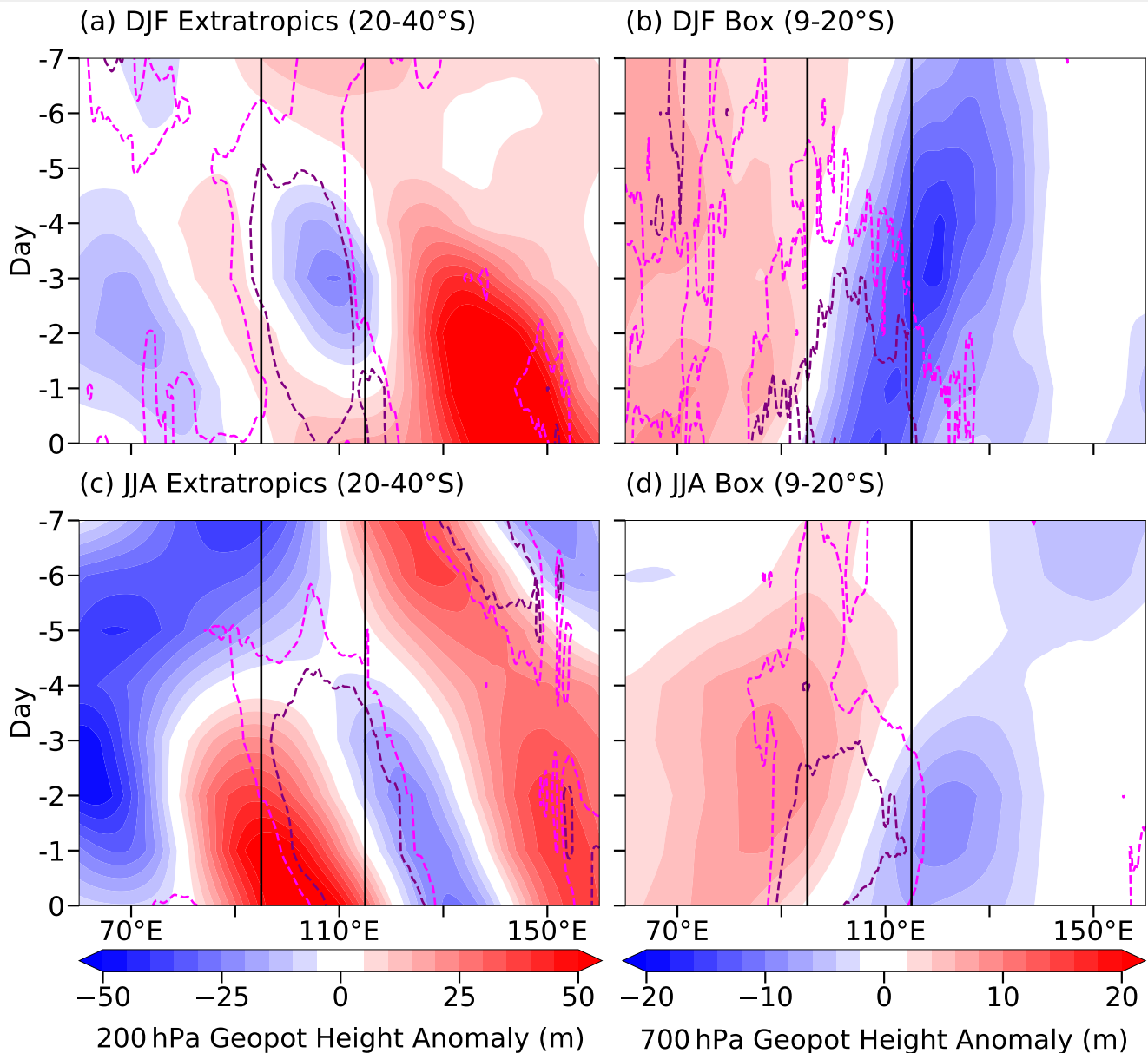


**Figure 7.** (a-b) Hovmöller plots of 200 hPa and 700 hPa geopotential height anomalies from Day -7 to 0 for the 47 dry events identified in DJF from 1979/80 to 2020/21. Anomalies at 200 hPa are averaged over an extratropical latitudinal transect from 20-40°S, and anomalies at 700 hPa are averaged over the latitudes of the box from 9-20°S. (c-d) are the same as in (a-b), except for the 56 dry events identified in JJA. Black lines represent the longitudinal limits of the identifier box as in Figure 2. For the extratropical panels (a and c), pink and purple dashed contours represent  $-0.005 \text{ Pa s}^{-1}$  and  $-0.010 \text{ Pa s}^{-1}$  vertical ascent anomalies respectively, therefore indicating regions of vertical descent. This is the same for the box panels (b and d), except the pink and purple contours represent  $-0.010 \text{ Pa s}^{-1}$  and  $-0.020 \text{ Pa s}^{-1}$  vertical anomalies respectively instead.

are observed to the east of the intrusion, tilted in a direction paralleling the trajectory of dry air.

### 3.3. Association with Modes of Variability

While the previous section established the identified dry events are associated with extratropical dry air intrusions, anomalous circulations unique to DJF and JJA acted as key regulatory mechanisms. These circulations could be due to the state of the large-scale environment as modulated by modes of variability. ~~Though the core aim of this research is not to establish links between dry air intrusions and these modes, we briefly analyse potential interactions.~~ Data for indices representing these modes

is used to determine associations between dry events and larger-scale controls.

ENSO Ocean Niño Index (ONI) data is available through the NOAA National Weather Service Climate Prediction Center. This data is derived from the 3-month average temperature anomaly in the surface waters of the central-eastern tropical Pacific. El Niño events are defined where  $\text{ONI} \geq 0.5^\circ\text{C}$  for 5 successive months, and La Niña events are defined where  $\text{ONI} \leq -0.5^\circ\text{C}$  for 5 successive months. IOD Dipole Mode Index (DMI) data is derived in a similar fashion to ENSO ONI data, with monthly DMI data available through the NOAA Earth System Research Laboratories

Physical Sciences Laboratory. DMI represents the anomalous sea-surface temperature gradient between the western equatorial and southeastern equatorial Indian Ocean. Positive IOD events are defined where  $DMI \geq 0.4^{\circ}\text{C}$  for 3 successive months. Negative IOD events are defined where  $DMI \leq -0.4^{\circ}\text{C}$  for 3 successive months. Both ONI and DMI values are available as monthly data.

MJO phase and amplitude is determined using RMM1 and RMM2 (Real-time Multivariate MJO series 1 and 2) data, available for each day. RMM1 and RMM2 are the principal components of the two leading empirical orthogonal functions (EOFs), defined by EOF analysis of the combined field of outgoing longwave radiation and wind, which define the phase of the MJO (Wheeler and Hendon, 2004). The amplitude is defined as  $\sqrt{RMM1^2 + RMM2^2}$  - an MJO event is when the amplitude for a specific day exceeds or is equal to 1.

Dry events were grouped into associations with phases of ENSO, IOD and MJO, as shown in Table 1 under columns labelled 'Freq'. As MJO phases can be associated with different geographical regions within the tropics, we employ the convention used in Wheeler and Hendon (2004) to group pairs of phases together. Where the MJO amplitude is below 1, we label an event as being under 'Phase 0'. No association with ENSO is observed. Links with IOD are possible in primarily JJA (17.9% of events) and potentially DJF (4.3%) in the positive state. These are however dwarfed by the proportion of events in the neutral phase (95.7% and 76.8% in DJF and JJA respectively). While the greatest proportion of events are found in 'Phase 0' of the MJO (29.8% and 42.9% in DJF and JJA respectively), dry events can be associated with Phases 6-7 and 8-1 in DJF (27.7% and 23.4% respectively) and Phases 2-3 in JJA (21.4%) where the MJO signal is strong.

These frequencies were normalised by dividing the fraction of events in each phase relative to the total number of events per season, by the fraction of days in each phase relative to the total number of days in each season across the 42 years. This calculation provides a ratio between event frequency and day frequency with respect to each phase. If this ratio equals 1, then the distribution of events in the phase is similar to picking randomly from all days in the season. If the ratio tends towards 2, it is twice as likely that the distribution of events is linked

to a phase compared to random selection, and therefore there is a potential relationship with the large-scale modes of variability. These values are found under columns in Table 1 labelled 'Norm'. As shown for both DJF and JJA, there is potential for association with the positive IOD (1.79 and 1.25 respectively). ENSO shows no relationship with either season. However, Phases 6-7 and 8-1 of the MJO for DJF (1.29 and 1.98 respectively) and Phases 2-3 and 4-5 for JJA (1.41 and 1.25 respectively) show tendency towards a relationship.

The statistical significance of these links were tested through bootstrapping. For each season (3791 and 3864 days for DJF and JJA respectively), we randomly subset a set of days of equivalent length to the number of events identified per season (47 and 56 for DJF and JJA respectively), where the state of each mode for each day is determined. We perform the normalisation calculations as described previously for these sets of days, relative to the distribution of days in the whole season across the phases of each mode. This process is repeated 1000 times to produce a distribution of ratios for the state of each mode for each season. Percentiles for values provided in the 'Norm' columns in Table 1 relative to the bootstrapped distribution are calculated to determine the significance of association with modes of variability. These percentiles are found in columns labelled 'P'tile'.

No associations between dry events and the state of ENSO in either season is found. Dry events are however more likely in the positive state of the IOD (72.4% and 82.0% in DJF and JJA respectively), but this is not statistically significant. The MJO on the other hand shows statistically significant links with dry events in each season. In DJF, dry events are significantly more likely in Phases 8-1 (99.6%) when the active phase of the MJO is away from the MC and likely in Phases 4-5 and Phases 6-7 (73.4% and 79.7% respectively) when the active phase is over or to the east of the MC. Dry events are also significantly less likely to occur in Phases 2-3 of the MJO (0.3%), when the active phase is just to the west of the MC over the Indian Ocean. In JJA, opposite results are observed. Dry events are significantly more likely in Phases 2-3 and Phases 4-5 (96.0% and 97.1% respectively), when the active phase of the MJO is over the Indian Ocean or MC. These events are also significantly less likely to happen when the active

Table 1. Dry event frequency (Freq) for both DJF and JJA across the states of each mode of variability analysed. Provided are ratios indicating the normalised event frequencies with respect to the number of days within each season associated with each state of each mode (Norm) and the percentiles these values represent when compared to the distribution of 1000 bootstrapped samples (P'tile). MJO phases are associated with geographical locations as follows: Phases 2 and 3 (Indian Ocean), Phases 4 and 5 (Maritime Continent), Phases 6 and 7 (West Pacific), Phases 8 and 1 (Western Hemisphere and Africa), as per Wheeler and Hendon (2004). Phase 0 represents times when the MJO amplitude is below 1 and therefore weak.

Mode	State	DJF (Freq)	DJF (Norm)	DJF (P'tile)	JJA (Freq)	JJA (Norm)	JJA (P'tile)
ENSO	El Niño	16	1.04	53.4 %	12	1.08	56.0 %
	Neutral	15	0.94	43.7 %	31	0.94	25.2 %
	La Niña	16	1.02	59.9 %	13	1.08	58.1 %
IOD	Positive	2	1.79	72.4 %	10	1.25	82.0 %
	Neutral	45	1.01	48.6 %	43	0.98	41.8 %
	Negative	0	0.00	11.1 %	3	0.75	44.1 %
MJO	Phase 0	14	0.87	16.7 %	24	0.99	26.2 %
	P2 and P3	2	0.27	0.3 %	12	1.41	96.0 %
	P4 and P5	7	0.90	73.4 %	8	1.25	97.1 %
	P6 and P7	13	1.29	79.7 %	7	1.04	47.3 %
	P8 and P1	11	1.98	99.6 %	5	0.50	2.4 %

phase of the MJO is away from the MC in Phases 8-1 (2.4 %). Therefore, there appears to be seasonal differences in associations between dry event occurrence and phase of the MJO.

### 3.4. Impact on Rainfall

In this section, we analyse the ~~impacts reductions in~~ mid-level humidity ~~have~~ on regional rainfall patterns. We use the dry events that take place in the available GPM data record from 2000/01 to 2019/20, providing 25 and 27 dry events for DJF and JJA respectively. Precipitation anomalies associated with each event are averaged, and then normalised with respect to the mean rainfall rate at that grid point per season (Figure 1b-c). Figure 8 shows these normalised anomalies, binned in groups of days relative to the event, averaged over smaller bin sizes closer to Day 0.

During DJF dry events, negative rainfall anomalies develop in the southern portion of the box NW of Australia up to 6-10 days before the dry event (Figure 8a). ~~These anomalies propagate north to northeastward from the southwest along with negative anomalies in specific humidity (maroon dashed contours) between Days -5 to -2, and the most intense rainfall anomalies coinciding with the most negative humidity anomalies~~ (Figure 8b). Positive anomalies in normalised precipitation rate, tilted SW-NE, are observed to the east of the dry anomaly. Around the time of the dry event, positive rainfall anomalies dissipate, but continued northward propagation of dry air coincides with decreases in rainfall with strongest reductions at the core of the dry anomaly,

south of Java (Figure 8c). Anomalies within the box near to the MC dissipate and disperse after the dry event. These ~~propagate~~ westward towards the Indian Ocean with the humidity anomaly, but a portion of rainfall reductions move (north)eastward (Figure 8d). Here, negative rainfall anomalies are observed over the ~~Lesser Sundas and the neighbouring Flores and Banda seas~~. Between Days +6 and +10, most of the negative rainfall and humidity anomalies have dissipated, though more localised dry air and reduced rainfall signatures persist (Figure 8e).

For JJA dry events, there are widespread pre-existing anomalies of reduced rainfall across the region up to 6-10 days prior to the dry event (Figure 8f). These span northwestern Australia, the shallow seas of the southern MC and some of the neighbouring islands. This pre-existing anomaly leads to ~~reductions over Java, the Lesser Sundas, south Sulawesi, and the Java and Flores Seas~~ 2-5 days before the dry event (Figure 8g). However, anomalies originating from the south, linked to the study region, are now observed along with negative specific humidity anomalies just to the northwest of Australia. Increases in rainfall are noted to the east over Australia. Widespread reductions in rainfall, coinciding with the humidity anomalies, are observed around the time of the dry event (Figure 8h). The pre-existing anomaly from the east leads to reductions over Java, south Sumatra, south Borneo and neighbouring seas. The rainfall anomaly from the south moves northwest towards the Indian Ocean with the reductions in humidity. Positive rainfall anomalies develop to the east of the dry anomaly over the Lesser Sundas and northern

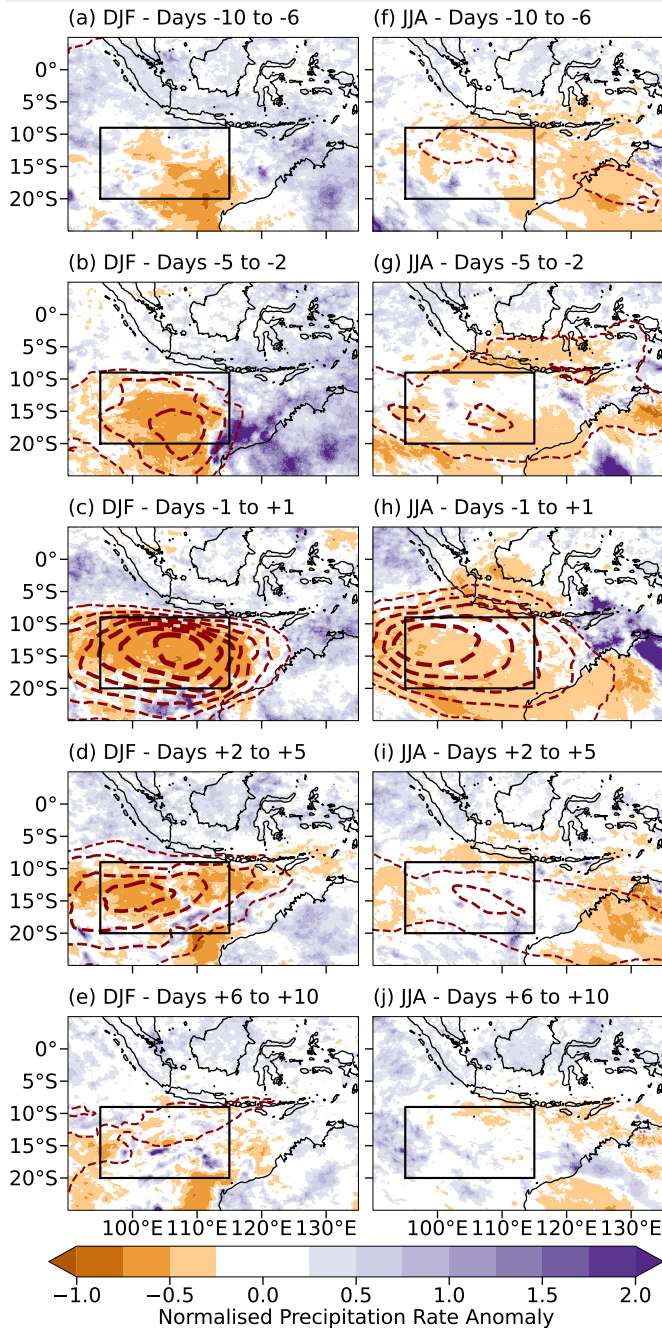


**Figure 8.** Normalised precipitation rate anomalies with respect to the mean rainfall for dry events in (a-e) DJF and (f-j) JJA within the available GPM record from 2000/01 to 2019/20 (25 for DJF and 27 for JJA), for Days -10 to +10. These have been binned into sets of days, with smaller bins closer to the dry event or Day 0, which each set of data is averaged over. Maroon dashed contours represent negative specific humidity anomalies averaged over these events, where increases in contour thickness reflect decreases (becoming more negative) in the mean specific humidity anomaly by  $0.5 \text{ g kg}^{-1}$ , starting at  $-0.5 \text{ g kg}^{-1}$ . The black box represents the domain used for identifying dry events as in Figure 2.

Australia, with a NW-SE tilt. Both negative and positive rainfall anomalies dissipate over the region up to 5 days after the dry event (Figure 8i). Some anomalies shift westward and southeast towards Australia where there are more intense reductions in rainfall, matching the trajectory of the humidity anomalies. After Day +6, observed anomalies dissipate (Figure 8j).

#### 4. Discussion

As shown in Sections 3.1 and 3.2, analysis of parcel trajectories and precursor regulatory mechanisms showed that air parcels associated with dry events can be attributed to dry air intrusions, originating from upper-level disturbances along the subtropical jet (Figures 3-7). These processes which are akin to Rossby wave breaking, as indicated in past studies (e.g. Numaguti, 1995; Funatsu and Waugh, 2008). Parallels can also be made in terms of dry air sourcing and pathways leading up to a dry event as seen in Feng et al. (2021). This work extends Feng et al. (2021)'s observations across a greater time period of analysis for more events, highlighting that events are inherently unique, as shown by the range in trajectory characteristics (Figures 3-4).

Pre-existing dry air anomalies observed coming from the east in JJA (Figure 6) are suggestive of links with Rossby wave breaking processes away from the region of analysis, resulting in dry air intrusions. Studies such as Casey et al. (2009) highlight that these processes take place more often in each hemisphere's winter. Figure 2 highlighted a high variance region in mid-level specific humidity between New Guinea and Australia. This may be the region of dry air sourcing prior to the analysed intrusions compared from the south over the Indian Ocean in JJA. Future work may involve repeating presented analysis, but using the region of high variance in the southeastern MC

Seasonal differences between dry events in DJF and JJA are, however, visible in terms of the mechanisms regulating their occurrence. Firstly, air parcels associated with dry air intrusions take less time to arrive into the tropics in JJA compared to DJF (Figures 3b-c and 3g), and those found in the domain up to 15 days prior to the dry event are located within more equatorial latitudes in JJA than in DJF (Figure 3a). This observation is likely to be a product of the northward migration of the subtropical jet and Intertropical Convergence Zone (ITCZ) during the austral winter, as well as strengthening of the jet stream, leading to faster advection of air parcels. However, any tropical sources of air parcels are most likely a mere product of the width of the box,  $\mathcal{O}(1000 \text{ km})$ , compared to the width of an average dry air intrusion,  $\mathcal{O}(10-100 \text{ km})$  (e.g. Raveh-Rubin, 2017). Therefore, not

all air parcels within the box for a given dry event would be directly linked to the intrusion.

Secondly, shifting of the jet northward in JJA is likely to be altering the direction of dry air trajectories into the MC from southerly to southeasterly, with changes to geopotential height anomalies noted. Past studies have found links between jet characteristics and resultant trajectories of dry air intrusions (e.g. Homeyer and Bowman, 2013). However, the more dominant regulatory trough (slightly dominant ridge) signature in DJF (JJA) may be a result of the events which have been composited. The eventual NW-SE tilt attributed to the mid-level trough anomalies in the region of the dry anomaly around Day 0 (Figures 5c and 6c) is an expected result due to anticyclonic shear on the equatorward flank of the intrusion/geopotential anomaly, as highlighted by Knippertz (2007).

Thirdly, the most pronounced differences are in forward trajectories associated with dry events themselves. As shown in Figures 3g and 4e-h, DJF air parcels have a greater signal of re-ascent after the dry event, suggestive of entrainment in convection within the tropics, compared to that in JJA. In addition to these observations, JJA air parcels are advected towards the Indian Ocean, with some further northeast from this position up to mainland Southeast Asia, compared to DJF where there is dominantly eastward advection towards New Guinea, and some advection westward towards the Indian Ocean (Figures 3d-f). The first association is that the lower-level (850 hPa) climatological wind field, provided in Figures 1b, characteristic of the monsoon circulation in each season suggest mean westerly motion in the lower-levels in DJF across the southern-central MC, with easterlies slightly further south, while still within the box latitudes (up to 20°S). This explains the largely eastward propagation of air parcels in DJF after continued descent below 700 hPa. Figure 1c, on the other hand, shows the opposing monsoon circulation for JJA, where there are strong low-level mean easterlies across the southern MC, which would explain the largely westward advection of parcels. To the northwest of the MC into the Indian Ocean near to the Bay of Bengal and mainland Southeast Asia, low-level monsoon circulation reverses from northeasterly (as in DJF) to southwesterly, providing reasoning for eventual advection of air parcels towards the mainland. Parcels, therefore, which

continue descent after the dry event will likely be entrained in the mean monsoon low-level circulation, influencing their eventual trajectory.

Impacts on rainfall generally follow the trajectories presented in this research, as shown in Figure 8. In both seasons, dry air coming from the extratropics suppresses rainfall over the ocean in the identifier box. This result agrees with the results from campaigns such as TOGA COARE over the tropical west Pacific (e.g. Parsons et al., 2000). In DJF, dry air propagates eastward, resulting in a suppressed rainfall signal over the Lesser Sundas of Indonesia, and neighbouring seas after the dry event (Figure 8d). In JJA, rainfall reductions over the islands of the MC are linked to the pre-existing dry air from a previous dry air intrusion originating from the east (Figures 9f-h). This observation supports the possibility of a greater frequency in dry air intrusions in the austral winter. As JJA trajectories are largely (north)westward, no further reductions over the MC can be attributed to the studied dry events, though rainfall suppression is apparent going into the eastern Indian Ocean (Figures 9h-i).

An increase in rainfall to the east of the dry anomalies, which have a tilt paralleling that of the dry air trajectory itself, was also observed (e.g. Figures 9b and 9g-h). When analysing key mechanisms regulating dry events (Figures 5-6), there was flow to the extratropics at both mid-levels and upper-levels to the east of troughs, resulting in increases in mid-level specific humidity. Such moist anomalies are found in similar positions to the positive rainfall anomalies in Figure 8 (over northwestern and northern Australia, as well as the Lesser Sundas), implying that roughly at the time of a dry event, it is possible to get increases in rainfall just to the east. This is an observation that Berry and Reeder (2016) found, where Australian summertime monsoon bursts took place to the east of an upper-level trough. Several authors have associated amplification of upper-level troughs with enhanced convection at the edges and to the east of descending dry air masses, thereby steering convection (e.g. Tompkins, 2001; Pohl et al., 2009; de Vries et al., 2016). Dry air intrusions and the associated disturbances themselves are driving the flow of moist air necessary to form convection, observed in past studies such as Knippertz (2007) and Ward et al. (2021) over Africa.

~~Though not the core aim of this work,~~ our investigation into associations between dry events and large-scale modes of variability (Table 1) found no link between ENSO and dry event occurrence. Berry and Reeder (2016), for example, also found no significant link between upper-level troughs, which regulate Australian summertime monsoon bursts, near to the study region, and ENSO. Pohl et al. (2009) found the opposite results for southern Africa, suggestive of global variability in associations between upper-level disturbances and ENSO. However, there are potential links with the positive IOD and dry event occurrence. During the positive IOD, high and low SSTs are observed in the western and eastern Indian Ocean respectively, with the converse applying to the negative IOD (e.g. Saji et al., 1999; Saji and Yamagata, 2003). These SSTs produce a Walker-like circulation with enhanced easterlies across the the Indian Ocean during the positive IOD, leading to enhanced descent over the MC and uplift over eastern Africa. As dry events are observed to be driven by vertical descent from the upper-levels (e.g. Figures 3g and 7a-b), greater association with this phase of the IOD is not surprising. Given the IOD develops in the austral winter (JJA) and peaks in the spring (SON), our results support a slightly greater likelihood of occurrence in the correct season. However, these results are not statistically significant.

In contrast with ENSO and IOD, significant links with the MJO have been noted. For DJF, it was observed that dry events are significantly more (less) likely when the MJO active phase is over the Western Hemisphere and Africa (Indian Ocean to the west of the MC), with non-significant links with increased likelihood when over the MC. For JJA, we find that when the active phase is over the Indian Ocean or MC (the Western Hemisphere and Africa), dry events are significantly more (less) likely. In more condensed terms, when the MJO active phase is in the vicinity of the region, dry events are more (less) likely in JJA (DJF), and the opposite when the MJO active phase is away from the region. Therefore, we find similar results to Berry and Reeder (2016) for DJF (JJA was not examined in their work). We hypothesise this is largely due to circulations which are driven by the large-scale tropical environment, most dominantly regulated by the MJO on intraseasonal timescales (Madden and Julian, 1971, 1972, 1994), which may be a product of equatorial

wave theory associated with MJO dynamics (e.g. Hendon and Salby, 1994; Maloney and Hartmann, 1998; Matthews, 2000). During the active phase, a tongue of low pressure strengthens to the east, associated with a Kelvin wave, with pressure troughs to the northwest and southwest, associated with Rossby waves (Matsuno, 1966; Gill, 1980). The opposite is observed for the suppressed phase of the MJO. The potential for dry air intrusion trajectories to be modified by Rossby waves has been past researched over the Indian Ocean in the Dynamics of the MJO (DYNAMO) field campaign (Kerns and Chen, 2014; Chen et al., 2016). Their observations included a strong MJO event and dry air intrusions over the Indian Ocean. A noted interaction linked dry air intrusions to westward-propagating synoptic Rossby gyres in the active envelope. These gyres induced low-level wind circulations drawing the dry air eastward into the equatorial region west of the envelope, contributing to a 1-2 day break in the rainfall during the MJO active phase, favouring a transition to the suppressed phase. This interaction was validated in various simulations (Wang et al., 2015; Kuznetsova et al., 2019).

Mid-level westerly anomalies persist over the southern MC in DJF (Figure 5), linked to the enhanced negative geopotential height anomaly and cyclonic circulation over northwestern Australia. With the strengthened mid-level trough in DJF enhancing both vertical descent of dry air from upper-levels (Figure 7b), and equatorward and eastward advection, a similar interaction to that in Kerns and Chen (2014) may be taking place. When the active phase of the MJO is over or to the east of the MC, westward-propagating cyclonic Rossby gyres, using the terminology of Kerns and Chen (2014), may be present near the region of study, which would enhanced westerly flow. In the opposite phases, with reversals of anomalous gyre circulations associated with the MJO, there may be easterly intensification, which is the reason for such air parcels propagating westward (e.g. Figures 3d-f). In JJA, opposite anomalies are noted, though mid-level easterlies are not as persistent (Figure 6) as the westerlies observed in DJF, likely linked to the anomalous geopotential signature being weaker (Figures 7c-d). With dry events more likely when the active phase of the MJO is to the west or over the MC, mid-level ridges are to have greater prevalence in the vicinity of the region linked with the suppressed phase of the MJO being



further to the east. There may be easterly intensification towards the Indian Ocean due to the anticyclonic circulation characteristic of these ridges. Therefore, MJO phase may have a control on both mid-level circulation (Figures 5-6) and geopotential (Figure 7) characteristics noted in each season. Precise details on the influence of the MJO and whether they influence circulation and geopotential anomalies regulating dry air intrusions are beyond the scope of this research and would require filtering of the MJO signal in relation to these events. The extent to which dry air intrusions and background modes of variability interact must also be spatially and temporally variable, so assumptions on their interactions over the MC cannot be made.

While the presented results have provided great insight into the mechanisms regulating dry event (or intrusion) occurrence, and their impacts on rainfall, we are limited by the fairly low sample size in terms of number of dry events per season, identified using the employed method. This is even though 42 years of data has been sampled. In particular, there are few events for analysing impacts on MC rainfall, with only 25 and 27 events analysed during DJF and JJA (for 20 years). Therefore, more events are required to provide confirmation of statistically significant links between dry events and the precursor regulatory mechanisms, processes that modulate their trajectories, and also their impacts on rainfall. All three of these links are potentially more visible on finer timescales, so will need further analysis beyond what has been achieved here, involving case study analysis.

## 5. Conclusion

In this work, we have used a normalised mid-level specific humidity metric to identify dry events south of the Maritime Continent in DJF and JJA. Processes controlling dry event occurrence and their impacts on rainfall are presented schematically in Figures 9a and 9b for DJF and JJA respectively. Air parcels associated with dry events in both seasons originate from the extratropics in the southern Indian Ocean as shown by back trajectory analysis, 5-10 days prior to the dry event. These air parcels are associated with synoptic mid-level dry air intrusions regulated by amplification of upper-level disturbances, linked to Rossby wave breaking, along the subtropical jet up to 5 days before the dry event. Descent of dry air takes place to the west of the upper-level trough and

east of the ridge. DJF intrusions are dominated by southerly mid-level advection and a mid-level cyclonic circulation anomaly (trough) northwest of Australia, whereas JJA intrusions have slight southeasterly flow of dry air from the extratropics due to a mid-level anticyclonic circulation anomaly (ridge) northwest of Australia. The circulation anomaly in DJF enhances westerlies in the southern Maritime Continent, allowing advection further east. In contrast, the anomaly in JJA enhances easterlies to the west, enabling westward advection. There are interactions between the low-level monsoon circulation in JJA, where northeasterly flow in DJF near mainland Southeast Asia and the Bay of Bengal reverses to southwesterly, directly air parcels further northward. Opposing tropical-extratropical flow to the east of intrusions in both seasons transports moisture over Australia and the Lesser Sundas. While, in both seasons, dry air intrusions descend from around 10 days before the event to 10 days after, eventual re-ascent is driven by entrainment into convection within the ITCZ in DJF, with continued low-level flow in JJA. Further northward propagation of air parcels into the JJA ITCZ is believed to enable similar re-ascent. Transport mechanisms, influenced by circulation and geopotential anomalies, attributable to dry air intrusion occurrence may be linked to modes of variability, primarily the MJO and potentially the IOD. However, assumptions cannot be made given this is beyond the scope of this work.

Dry air coming from the extratropics suppresses rainfall, supporting work from other studies analysing convective suppression in the tropics linked to dry air intrusions. Rainfall suppression signatures largely follow intrusion trajectories, where in DJF, reduced rainfall may be found in the southern Maritime Continent over the Lesser Sundas and neighbouring seas, following the eastward propagation. JJA, on the other hand, has limited rainfall reductions over the southern Maritime Continent linked to analysed intrusions. Instead, dry air originating from further east, suggestive of Rossby wave breaking elsewhere (enhanced in the wintertime), leads to reductions over Java, Sumatra, southern Borneo and neighbouring seas. Anomalies linked to the intrusion propagate to the Indian Ocean. In both cases, reduced rainfall can be seen developing around 5 days prior to up to 5 days after the dry event. In addition, signatures of positive rainfall anomalies are found to the east

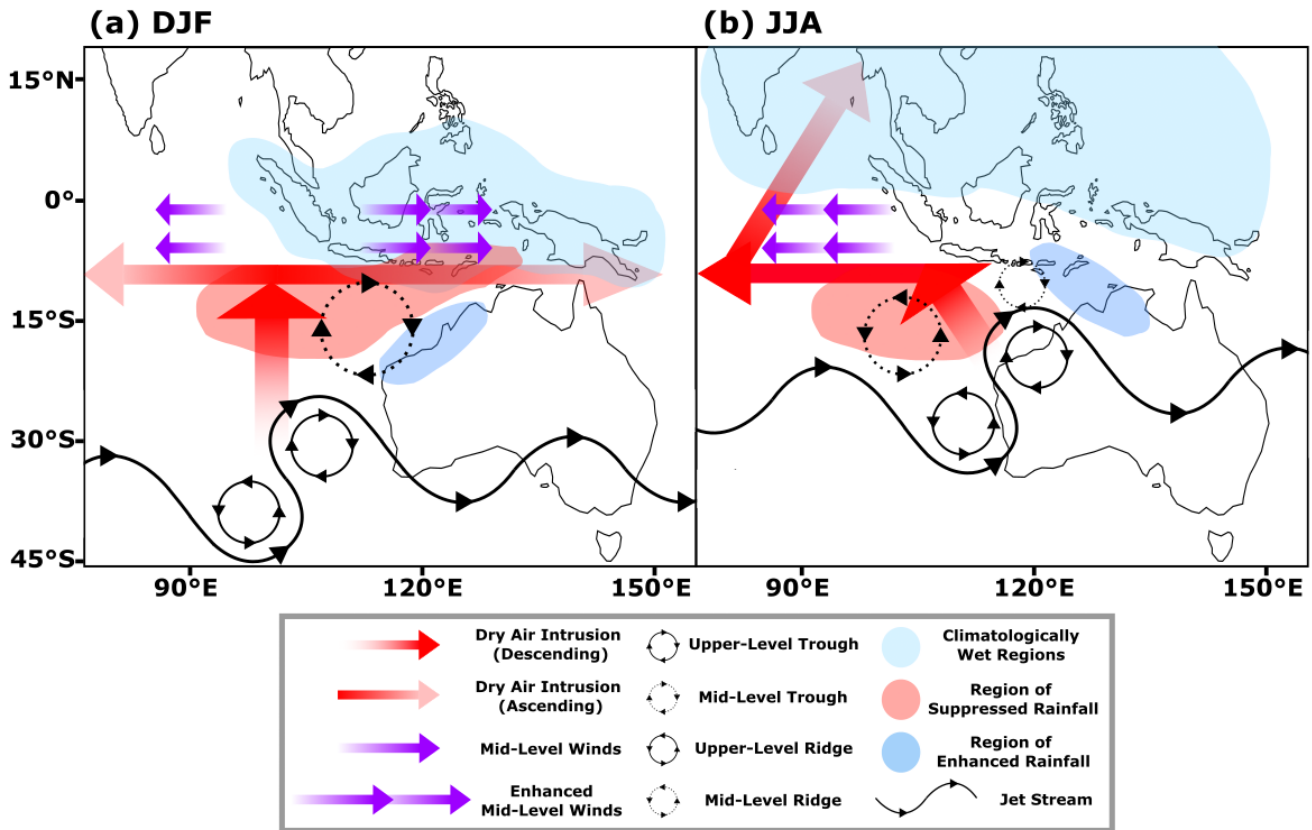


**Figure 9.** Schematic showing the processes regulating the occurrence of dry events, due to extratropical mid-level dry air intrusions, to the south of the Maritime Continent, and their impacts on Maritime Continent rainfall, for (a) DJF and (b) JJA. Arrow size is not representative of intrusion characteristics - they merely represent direction and vertical motion.

of the dry anomalies, indicative of enhanced convection linked to convergence of moist air coming from the tropics to the extratropics encountering the eastward propagation of upper-level disturbances and the dry signals. These have been observed elsewhere in the tropics.

While this work has extended observations made in past work through usage of larger datasets, this approach requires further validation from case study analysis of events linked to dry air intrusions. This will reveal the finer details on what controls their occurrence, and their impacts on convection and rainfall over the Maritime Continent. Impacts originating from both the abrupt pauses in convection, enabling recharge in BL moisture, and also enhanced rainfall/steering of convection on margins through dynamical uplift and low-level interactions, are critical to understand. Future work should involve incorporation of both reanalysis and model data, as this will allow testing of the representation of synoptic processes such as dry air intrusions in global and regional simulations, while increasing our understanding of the associated mechanisms particularly over the Maritime Continent. These include interactions with

the climatological mean circulation, as well as potentially large-scale modes of variability. Regardless, our work has provided insight into key processes and impacts linked to dry air intrusions (in terms of both rainfall suppression and enhancement), supporting and expanding on past studies. Improving our general understanding of Maritime Continent precipitation patterns will provide benefits for forecasting and issuing severe weather warnings, as well as validation of numerical weather prediction models. Any improvements to regional systematic biases and our understanding of more complex processes too will ultimately contribute to improved situational awareness for local agencies, decision makers, and communities.

### Acknowledgements

Funding for this research was provided by NERC through a SENSE CDT studentship (NE/T00039X/1). Additional thanks go to John Marsham, Amanda Maycock, and researchers involved in the TerraMaris project for their input.

## References

- Ahmed, F. and Neelin, J. D. (2021). Protected convection as a metric of dry air influence on precipitation. *Journal of Climate*, **34**, 3821–3838.
- Appenzeller, C. and Davies, H. (1992). Structure of stratospheric intrusions into the troposphere. *Nature*, **358**, 570–572.
- Berry, G. J. and Reeder, M. J. (2016). The dynamics of Australian monsoon bursts. *Journal of the Atmospheric Sciences*, **73**, 55–69.
- Birch, C. E., Webster, S., Peatman, S. C., Parker, D. J., Matthews, A. J., Li, Y. and Hassim, M. E. (2016). Scale interactions between the MJO and the western Maritime Continent. *Journal of Climate*, **29**, 2471–2492.
- Bithell, M., Gray, L. J. and Cox, B. D. (1999). A Three-Dimensional View of the Evolution of Midlatitude Stratospheric Intrusions. *Journal of the Atmospheric Sciences*, **56**, 673–688.
- Brown, R. G. and Zhang, C. (1997). Variability of Midtropospheric Moisture and Its Effect on Cloud-Top Height Distribution during TOGA COARE\*. *Journal of the Atmospheric Sciences*, **54**, 2760–2774.
- Browning, K. A. (1997). The dry intrusion perspective of extra-tropical cyclone development. *Meteorological Applications*, **4**, 317–324.
- Casey, S. P. F., Dessler, A. E. and Schumacher, C. (2009). Five-year Climatology of Midtroposphere Dry Air Layers in Warm Tropical Ocean Regions as viewed by AIRS/Aqua. *Journal of Applied Meteorology and Climatology*, **48**, 1831–1842.
- Chen, S. S., Kerns, B. W., Guy, N., Jorgensen, D. P., Delanoč, J., Viltard, N., Zappa, C. J., Judt, F., Lee, C. Y. and Savarin, A. (2016). Aircraft Observations of Dry Air, the ITCZ, Convective Cloud Systems, and Cold Pools in MJO during DYNAMO. *Bulletin of the American Meteorological Society*, **97**, 405–423.
- Danielsen, E. F. (1968). Stratospheric-Tropospheric Exchange Based on Radioactivity, Ozone and Potential Vorticity. *Journal of the Atmospheric Sciences*, **25**, 502–518.
- Deng, K., Yang, S., Ting, M., Hu, C. and Lu, M. (2018). Variations of the mid-Pacific trough and their relations to the Asian-Pacific-North American climate: Roles of tropical sea surface temperature and Arctic sea ice. *Journal of Climate*, **31**, 2233–2252.
- Dixon, M. A., Thorpe, A. J. and Browning, K. A. (2003). Layer-wise attribution of vertical motion and the influence of potential-vorticity anomalies on synoptic development. *Quarterly Journal of the Royal Meteorological Society*, **129**, 1761–1778.
- Draxler, R. R., Spring, S., Maryland, U. S. A. and Hess, G. D. (1998). An Overview of the HYSPLIT-4 Modelling System for Trajectories, Dispersion, and Deposition. *Australian Meteorological Magazine*, **47**, 295–308.
- Fauzi, R. R. and Hidayat, R. (2018). Role of cold surge and MJO on rainfall enhancement over Indonesia during East Asian winter monsoon. *IOP Conference Series: Earth and Environmental Science*, **149**.
- Feng, L., Zhang, T., Koh, T. Y. and Hill, E. M. (2021). Selected Years of Monsoon Variations and Extratropical Dry-Air Intrusions Compared with the Sumatran GPS Array Observations in Indonesia. *Journal of the Meteorological Society of Japan*, **99**, 505–536.
- Ferrett, S., Yang, G. Y., Woolnough, S. J., Methven, J., Hodges, K. and Holloway, C. E. (2020). Linking extreme precipitation in Southeast Asia to equatorial waves. *Quarterly Journal of the Royal Meteorological Society*, **146**, 665–684.
- Fletcher, J. K., Parker, D. J., Hunt, K. M., Vishwanathan, G. and Govindankutty, M. (2018). The interaction of Indian monsoon depressions with northwesterly midlevel dry intrusions. *Monthly Weather Review*, **146**, 679–693.
- Fletcher, J. K., Parker, D. J., Turner, A. G., Menon, A., Martin, G. M., Birch, C. E., Mitra, A. K., Mrudula, G., Hunt, K. M., Taylor, C. M., Houze, R. A., Brodzik, S. R. and Bhat, G. S. (2020). The dynamic and thermodynamic structure of the monsoon over southern india: New observations from the INCOMPASS IOP. *Quarterly Journal of the Royal Meteorological Society*, **146**, 2867–2890.
- Funatsu, B. M. and Waugh, D. W. (2008). Connections between potential vorticity intrusions and convection in the eastern tropical Pacific. *Journal of the Atmospheric Sciences*, **65**, 987–1002.
- Gill, A. (1980). Some simple solutions for heat-induced tropical circulation. *Quart. J. R. Met. Soc.*, **106**, 447–462.
- Haylock, M. and McBride, J. (2001). Spatial Coherence and Predictability of Indonesian Wet Season Rainfall. *Journal of Climate*, **14**, 3882–3887.
- Hendon, H. H. and Salby, M. L. (1994). The Life Cycle of the Madden-Julian Oscillation. *American Meteorological Society*, **51**, 2225–2237.
- Hersbach, H., Bell, B., Berrisford, P., Hirahara, S., Horányi, A., Muñoz-Sabater, J., Nicolas, J., Peubey, C., Radu, R., Schepers, D., Simmons, A., Soci, C., Abdalla, S., Abellan, X., Balsamo, G., Bechtold, P., Biavati, G., Bidlot, J., Bonavita, M., Chiara, G. D., Dahlgren, P., Dee, D., Diamantakis, M., Dragani, R., Flemming, J., Forbes, R., Fuentes, M., Geer, A., Haimberger, L., Healy, S., Hogan, R. J., Hólm, E., Janisková, M., Keeley, S., Laloyaux, P., Lopez, P., Lupu, C., Radnoti, G., de Rosnay, P., Rozum, I., Vamborg, F., Villaume, S. and Thépaut, J. N. (2020). The ERA5 global reanalysis. *Quarterly Journal of the Royal Meteorological Society*, **146**, 1999–2049.
- Homeyer, C. R. and Bowman, K. P. (2013). Rossby wave breaking and transport between the tropics and extratropics above the subtropical jet. *Journal of the Atmospheric Sciences*, **70**, 607–626.
- Hoskins, B., Pedder, M. and Jones, D. W. (2003). The omega equation and potential vorticity. *Quarterly Journal of the Royal Meteorological Society*, **129**, 3277–3303.
- Huffman, G. J., Bolvin, D. T., Braithwaite, D., Hsu, K., Joyce, R., Kidd, C., Nelkin, E. J., Sorooshian, S., Tan, J. and Xie, P. (2020). Nasa Global Precipitation Measurement (GPM) Integrated Multi-satellitE Retrievals for GPM (IMERG) Algorithm Theoretical Basis Document (ATBD) Version 06.

- Ichikawa, H. and Yasunari, T. (2006). Time-Space Characteristics of Diurnal Rainfall over Borneo and Surrounding Oceans as Observed by TRMM-PR. *Journal of Climate*, **19**, 1238–1260.
- Jin, F. and Hoskins, B. J. (1995). The Direct Response to Tropical Heating in a Baroclinic Atmosphere. *Journal of the Atmospheric Sciences*, **52**, 307–319.
- Johnson, R. H., Ciesielski, P. E. and Cotturone, J. A. (2001). Multiscale Variability of the Atmospheric Mixed Layer over the Western Pacific Warm Pool. *Journal of the Atmospheric Sciences*, **58**, 2729–2750.
- Kerns, B. W. and Chen, S. S. (2014). Equatorial dry air intrusion and related synoptic variability in MJO initiation during DYNAMO. *Monthly Weather Review*, **142**, 1326–1343.
- Knippertz, P. (2007). Tropical-extratropical interactions related to upper-level troughs at low latitudes. *Dynamics of Atmospheres and Oceans*, **43**, 36–62.
- Krishnamurti, T. N., Thomas, A., Simon, A. and Kumar, V. (2010). Desert air incursions, an overlooked aspect, for the dry spells of the Indian summer monsoon. *Journal of the Atmospheric Sciences*, **67**, 3423–3441.
- Kumar, K. N., Phanikumar, D. V., Sharma, S., Basha, G., Naja, M., Ouarda, T. B., Ratnam, M. V. and kumar, K. K. (2019). Influence of tropical-extratropical interactions on the dynamics of extreme rainfall event: A case study from Indian region. *Dynamics of Atmospheres and Oceans*, **85**, 28–40.
- Kuznetsova, D., Dauhut, T. and Chaboureau, J. P. (2019). The Three Atmospheric Circulations over the Indian Ocean and the Maritime Continent and Their Modulation by the Passage of the MJO. *Journal of the Atmospheric Sciences*, **76**, 517–531.
- Li, D., Bian, J. C. and Fan, Q. J. (2015). A deep stratospheric intrusion associated with an intense cut-off low event over East Asia. *Science China Earth Sciences*, **58**, 116–128.
- Lucas, C. and Zipser, E. J. (2000). Environmental Variability during TOGA COARE. *Journal of the Atmospheric Sciences*, **57**, 2333–2350.
- Lucas, C., Zipser, E. J. and Ferrier, B. S. (2000). Sensitivity of Tropical West Pacific Oceanic Squall Lines to Tropospheric Wind and Moisture Profiles. *Journal of the Atmospheric Sciences*, **57**, 2351–2373.
- Madden, R. A. and Julian, P. R. (1971). Detection of a 40–50 Day Oscillation in the Zonal Wind in the Tropical Pacific. *Journal of the Atmospheric Sciences*, **28**, 702–708.
- (1972). Description of Global-Scale Circulation Cells in the Tropics with a 40–50 Day Period. *Journal of the Atmospheric Sciences*, **29**, 1109–1123.
- (1994). Observations of the 40–50-Day Tropical Oscillation — A Review. *Monthly Weather Review*, **122**, 814–837.
- Maloney, E. D. and Hartmann, D. L. (1998). Frictional Moisture Convergence in a Composite Life Cycle of the Madden-Julian Oscillation. *Journal of Climate*, **11**, 2387–2403.
- Mapes, B. E. and Zuidema, P. (1996). Radiative-Dynamical Consequences of Dry Tongues in the Tropical Troposphere. *Journal of the Atmospheric Sciences*, **53**, 620–638.
- Matsuno, T. (1966). Quasi-Geostrophic Motions in the Equatorial Area\*. *Journal of the Meteorological Society of Japan*, **44**, 25–43.
- Matthews, A. J. (2000). Propagation mechanisms for the Madden-Julian Oscillation. *Q. J. R. Meteorol. Soc.*, **126**, 2637–2651.
- Mori, S., Jun-Ichi, H., Yamanaka, M. D., Okamoto, N., Murata, F., Sakurai, N. and Hashiguchi, H. (2004). Diurnal Land-Sea Rainfall Peak Migration over Sumatera Island, Indonesian Maritime Continent, Observed by TRMM Satellite and Intensive Rawinsonde Soundings. *Monthly Weather Review*, **132**, 2021–2039.
- Murata, F., Yamanaka, M. D., Mori, S., Kudsy, M., Sribimawati, T. and Suhardi, B. (2006). Dry Intrusions Following Eastward-Propagating Synoptic-Scale Cloud Systems over Sumatera Island. *Journal of the Meteorological Society of Japan*, **84**, 277–294.
- Narulita, I. and Ningrum, W. (2018). Extreme flood event analysis in Indonesia based on rainfall intensity and recharge capacity. *IOP Conference Series: Earth and Environmental Science*, **118**.
- Neale, R. and Slingo, J. (2003). The Maritime Continent and Its Role in the Global Climate: A GCM Study. *Journal of Climate*, **16**, 834–848.
- Nugroho, Y. A., Fajarianti, R., Imami, A. F. and Winarso, P. A. (2019). Identification of The Influence of Long Winter Season in 2017–2018 to the Forming of Strong Northerly Cold Surge over West Indonesia. *IOP Conference Series: Earth and Environmental Science*, **303**.
- Numaguti, A. (1995). Characteristics of 4-to-20-Day-Period Disturbances Observed in the Equatorial Pacific during the TOGA COARE IOP. *Journal of the Meteorological Society of Japan*, **73**, 353–377.
- Parker, D. J., Willetts, P., Birch, C., Turner, A. G., Marsham, J. H., Taylor, C. M., Kolusu, S. and Martin, G. M. (2016). The interaction of moist convection and mid-level dry air in the advance of the onset of the Indian monsoon. *Quarterly Journal of the Royal Meteorological Society*, **142**, 2256–2272.
- Parsons, D. B., Yoneyama, K. and Redelsperger, J.-L. (2000). The evolution of the tropical western Pacific atmosphere-ocean system following the arrival of a dry intrusion. *Q. J. R. Meteorol. Soc.*, **126**, 517–548.
- Peatman, S. C., Matthews, A. J. and Stevens, D. P. (2014). Propagation of the Madden-Julian Oscillation through the Maritime Continent and scale interaction with the diurnal cycle of precipitation. *Quarterly Journal of the Royal Meteorological Society*, **140**, 814–825.
- Peatman, S. C., Schwendike, J., Birch, C. E., Marsham, J. H., Matthews, A. J. and Yang, G.-Y. (2021). A local-to-large scale view of Maritime Continent rainfall: control by ENSO, MJO and equatorial waves. *Journal of Climate*, **1–52**.
- Pohl, B., Fauchereau, N., Richard, Y., Rouault, M. and Reason, C. J. (2009). Interactions between synoptic, intraseasonal and interannual convective variability over Southern Africa. *Climate Dynamics*, **33**, 1033–1050.
- Qian, J. H. (2008). Why Precipitation Is Mostly Concentrated over Islands in the Maritime Continent. *Journal of the Atmospheric Sciences*, **65**, 1428–1441.

- Ramage, C. S. (1968). Role of a Tropical "Maritime Continent" in the Atmospheric Circulation. *Monthly Weather Review*, **96**, 365–370.
- Rauniyar, S. P. and Walsh, K. J. (2013). Influence of ENSO on the diurnal cycle of rainfall over the Maritime Continent and Australia. *Journal of Climate*, **26**, 1304–1321.
- Raveh-Rubin, S. (2017). Dry intrusions: Lagrangian climatology and dynamical impact on the planetary boundary layer. *Journal of Climate*, **30**, 6661–6682.
- Redelsperger, J.-L., Parsons, D. B. and Guichard, F. (2002). Recovery Processes and Factors Limiting Cloud-Top Height following the Arrival of a Dry Intrusion Observed during TOGA COARE. *Journal of the Atmospheric Sciences*, **59**, 2438–2457.
- Rodwell, M. J. (1997). Breaks in the Asian Monsoon: The Influence of Southern Hemisphere Weather Systems. *Journal of the Atmospheric Sciences*, **54**, 2597–2611.
- Ryoo, J.-M., Waugh, D. W. and Gettelman, A. (2008). Variability of subtropical upper tropospheric humidity. *Atmos. Chem. Phys*, **8**, 2643–2655.
- Saji, N., Goswami, B., Vinayachandran, P. and Yamagata, T. (1999). A dipole mode in the tropical Indian Ocean. *Nature*, **401**, 360–363.
- Saji, N. and Yamagata, T. (2003). Possible impacts of Indian Ocean Dipole mode events on global climate. *Climate Research*, **25**, 151–169.
- Scoccimarro, E., Gualdi, S., Bellucci, A., Peano, D., Cherchi, A., Vecchi, G. A. and Navarra, A. (2020). The typhoon-induced drying of the Maritime Continent. *PNAS*, **117**, 3983–3988.
- Seto, T. H., Yamamoto, M. K., Hashiguchi, H., Fukao, S., Abo, M., Kozu, T. and Kudsy, M. (2006). Observational Study on Westerly Wind Burst over Sumatra, Indonesia by the Equatorial Atmosphere Radar - A Case Study During the First CPEA Campaign. *Journal of the Meteorological Society of Japan*, **84A**, 95–112.
- Sheu, R.-S. and Liu, G. (1995). Atmospheric humidity variations associated with westerly wind bursts during Tropical Ocean Global Atmosphere (TOGA) Coupled Ocean Atmosphere Response Experiment (COARE). *Journal of Geophysical Research*, **100**, 25759–25768.
- Silverman, V., Nahum, S. and Raveh-Rubin, S. (2021). Predicting origins of coherent air mass trajectories using a neural network—the case of dry intrusions. *Meteorological Applications*, **28**.
- Simpson, J., Kummerow, C., Tao, W.-K. and Adler, R. F. (1996). On the Tropical Rainfall Measuring Mission (TRMM). *Meteorol. Atmos. Phys*, **60**, 19–36.
- Singh, R. and Sandeep, S. (2021). Dynamics of dry air intrusion over India during summer monsoon breaks. *Climate Dynamics*.
- Sprenger, M. and Wernli, H. (2015). The LAGRANTO Lagrangian analysis tool-version 2.0. *Geoscientific Model Development*, **8**, 2569–2586.
- Stein, A. F., Draxler, R. R., Rolph, G. D., Stunder, B. J., Cohen, M. D. and Ngan, F. (2015). NOAA's HYSPLIT Atmospheric Transport and Dispersion Modeling System. *Bulletin of the American Meteorological Society*, **96**, 2059–2077.
- Stohl, A. (2001). A 1-year Lagrangian "climatology" of airstreams in the Northern Hemisphere troposphere and lowermost stratosphere. *Journal of Geophysical Research Atmospheres*, **106**, 7263–7279.
- Tompkins, A. M. (2001). Organization of Tropical Convection in Low Vertical Wind Shears: The Role of Water Vapor. *Journal of the Atmospheric Sciences*, **58**, 529–545.
- Vaughan, G., Antonescu, B., Schultz, D. M. and Dearden, C. (2017). Invigoration and capping of a convective rainband ahead of a potential vorticity anomaly. *Monthly Weather Review*, **145**, 2093–2117.
- Vincent, C. L. and Lane, T. P. (2016). Evolution of the diurnal precipitation cycle with the passage of a Madden-Julian oscillation event through the Maritime Continent. *Monthly Weather Review*, **144**, 1983–2005.
- Volonté, A., Turner, A. G. and Menon, A. (2020). Air mass analysis of the processes driving the progression of the Indian summer monsoon. *Quarterly Journal of the Royal Meteorological Society*, **146**, 2949–2980.
- de Vries, A. J., Feldstein, S. B., Riemer, M., Tyrllis, E., Sprenger, M., Baumgart, M., Fnais, M. and Lelieveld, J. (2016). Dynamics of tropical-extratropical interactions and extreme precipitation events in Saudi Arabia in autumn, winter and spring. *Quarterly Journal of the Royal Meteorological Society*, **142**, 1862–1880.
- de Vries, A. J., Ouwersloot, H. G., Feldstein, S. B., Riemer, M., Kenawy, A. M. E., McCabe, M. F. and Lelieveld, J. (2018). Identification of Tropical-Extratropical Interactions and Extreme Precipitation Events in the Middle East Based On Potential Vorticity and Moisture Transport. *Journal of Geophysical Research: Atmospheres*, **123**, 861–881.
- Wang, S., Sobel, A. H., Zhang, F., Sun, Y. Q., Yue, Y. and Zhou, L. (2015). Regional Simulation of the October and November MJO Events Observed during the CINDY/DYNAMO Field Campaign at Gray Zone Resolution. *Journal of Climate*, **28**, 2097–2119.
- Ward, N., Fink, A. H., Keane, R. J., Guichard, F., Marsham, J. H., Parker, D. J. and Taylor, C. M. (2021). Synoptic timescale linkage between midlatitude winter troughs Sahara temperature patterns and northern Congo rainfall: A building block of regional climate variability. *International Journal of Climatology*, **41**, 3153–3173.
- Waugh, D. W. and Polvani, L. M. (2000). Climatology of intrusions into the tropical upper troposphere. *Geophysical Research Letters*, **27**, 3857–3860.
- Wernli, H. and Davies, H. C. (1997). A Lagrangian-based analysis of extratropical cyclones. I: The method and some applications. *Quarterly Journal of the Royal Meteorological Society*, **123**, 467–489.
- Wheeler, M. and Kiladis, G. N. (1999). Convectively coupled equatorial waves: Analysis of clouds and temperature in the wavenumber-frequency domain. *Journal of the Atmospheric Sciences*, **56**, 374–399.
- Wheeler, M. C. and Hendon, H. H. (2004). An All-Season Real-Time Multivariate MJO Index: Development of an Index for Monitoring and Prediction. *Monthly Weather Review*, **132**, 1917–1932.

- van der Wiel, K., Matthews, A. J., Stevens, D. P. and Joshi, M. M. (2015). A dynamical framework for the origin of the diagonal South Pacific and South Atlantic Convergence Zones. *Quarterly Journal of the Royal Meteorological Society*, **141**, 1997–2010.
- Wijayanti, P., Zhu, X., Hellegers, P., Budiyono, Y. and van Ierland, E. C. (2017). Estimation of river flood damages in Jakarta, Indonesia. *Natural Hazards*, **86**, 1059–1079.
- Yamanaka, M. D., Ogino, S. Y., Wu, P. M., Jun-Ichi, H., Mori, S., Matsumoto, J. and Syamsudin, F. (2018). Maritime continent coastlines controlling Earth's climate. *Progress in Earth and Planetary Science*, **5**.
- Yang, G.-Y., Hoskins, B. and Slingo, J. (2003). Convectively Coupled Equatorial Waves: A New Methodology for Identifying Wave Structures in Observational Data. *Journal of the Atmospheric Sciences*, **60**, 1637–1654.
- Yang, G.-Y. and Slingo, J. (2001). The Diurnal Cycle in the Tropics. *Monthly Weather Review*, **129**, 784–801.
- Yang, S., Cui, X. and Ran, L. (2009). Analyses of Dry Intrusion and Instability during a Heavy Rainfall Event that Occurred in Northern China. *Atmospheric and Oceanic Science Letters*, **2**, 108–112.
- Yokoi, S., Mori, S., Katsumata, M., Geng, B., Yasunaga, K., Syamsudin, F., Nurhayati and Yoneyama, K. (2017). Diurnal cycle of precipitation observed in the western coastal area of Sumatra Island: Offshore preconditioning by gravity waves. *Monthly Weather Review*, **145**, 3745–3761.
- Yoneyama, K. and Fujitani, T. (1995). The Behavior of Dry Westerly Air Associated With Convection Observed during the TOGA-COARE R/V Natsushima Cruise. *Journal of the Meteorological Society of Japan*, **73**, 291.
- Yoneyama, K. and Parsons, D. B. (1999). A Proposed Mechanism for the Intrusion of Dry Air into the Tropical Western Pacific Region. *Journal of the Atmospheric Sciences*, **56**, 1524–1546.
- Zachariasse, M., Smit, H. G., Velthoven, P. F. V. and Kelder, H. (2001). Cross-tropopause and interhemispheric transports into the tropical free troposphere over the Indian Ocean. *Journal of Geophysical Research*, **106**, 28441–28452.
- Zhang, C. (2005). Madden-Julian Oscillation. *Reviews of Geophysics*, **43**, 1–36.
- Zhang, C. and Chou, M.-D. (1999). Variability of Water Vapor, Infrared Radiative Cooling, and Atmospheric Instability for Deep Convection in the Equatorial Western Pacific. *Journal of the Atmospheric Sciences*, **56**, 711–723.